Part II

The oceanic numerical modeling of the eastern tropical Pacific Ocean

Chapter 4

The oceanic model

4.1 Introduction

The numerical modeling technique has been widely developed in recent years and used in an attempt to reproduce the operation and interaction of the basic elements of geophysical fluid dynamics in the natural environment. Then by comparing model predictions with experimental and observational data in the real world, scientists may seek to refine the underlying principles and routines of the model itself so as to enhance its value and relevance as the accuracy of the model is improved. In this manner, trustworthy numerical models become valuable tools in the service of the Science as they are elevated to a new role, in which they assume a capacity to validate theories and hypotheses. It is in this context that the following sections of this work present and describe an oceanic numerical approach developed so as to explore the influences of the atmospheric flow of freshwater as an independent variable of input to the SSS of the eastern tropical Pacific Ocean.

In the following stage of the study, a numerical modeling technique combines an association of the velocity fields along with temperature characteristics of the Modular Ocean Model (MOM) within a mixed layer model. Initially the intention had been to present this numerical approach as a complementary component of the earlier atmospheric studies and for this reason its detailed description and validation were not included but were relegated to this later chapter. This separation of justification and

focus was seen to impair the thrust of the numerical model input. There also transpired in the development of the earlier section, particularly in the lack of literature relating to some features of the salinity anomalies of the eastern tropical Pacific region, that the contribution of a numerical model might well have a much greater relevance in its own right, namely in a contribution to a general data bank of Pacific Ocean surface layer salinity either on spatial or temporal scales. This re-arrangement of order and treatment may be excused.

Restricting the focus to the eastern region of the Pacific Ocean, a very short summary of its main hydrodynamic features is presented as follows.

The circulation in the eastern Pacific Ocean is described by Kessler (2006), with a comprehensive review since the first descriptive attempts, dating back to the 1950's. Furthermore, the author gives an extensive description of the implications in the circulation due to wind jets that reach the eastern Pacific Ocean through three major gaps in the Central America cordillera (the Chivela Pass in the Isthmus of Tehuantepec in Mexico, the Lake District lowlands of Nicaragua inland of the Gulf of Papagayo, and the central isthmus of Panama where the Panama Canal was built). Their influences are felt as fluctuations of the thermocline depth, SST, and longitudinal migration in the ITCZ. Such fluctuations and seasonal variability might be attributed to the wind jets, but also perhaps to Rossby waves or Ekman pumping. The oceanic current system in the eastern Pacific Ocean, under the influence of the atmospheric ITCZ, is mainly comprised of four currents: South Equatorial Current (SEC), Equatorial Undercurrent (EUC), North Equatorial Current (NEC) and North Equatorial Counter Current (NECC). The region is strongly influenced by a cold tongue intrusion whereby the EUC loses volume through upwelling from successively denser layers (Sloyan *et al.*, 2003). In 2002, Johnson *et al.* carried out studies with data derived from Conductivity-Temperature-Depth (CTD) and Acoustic Doppler Current Profiler (ADCP) measurements across the Pacific. Johnson *et al.* (2002a) estimate the mean

current fields and oceanic properties, such as temperature and salinity fields, as well as their variability, seasonal cycle and linear correlation with the SOI.

On the foregoing basis, and mindful of the existing foundation of relevant knowledge accumulated by other authors, there is a conviction that an hydro-dynamical layered numerical model might well assist the investigation of salinity in the upper layers of the eastern tropical Pacific. By definition almost, such a model will need to be of mixed layer type, will need to be developed and justified by a validation phase using available environmental data in the first instance, and then to be extended by a staged and more general reproductive application to the relevant published work. Only then will it be possible to experiment with the potential of the model to expand existing knowledge in its own right. Thus, when these sections will be finished, in addition to the previous atmospheric studies presented in Part I, it is expected that they will form an enhanced understanding of the properties and their interaction within the eastern Pacific Ocean in one and the same work.

4.2   The numerical ocean modeling

The oceanic numerical model, as already initially introduced in Part I, and now to be developed and validated, represents an association of hydrodynamic and mixed layer principles which together have the potential to qualify for recognition as an "Active Tracer Model" (ATM).

The conceived ATM combines a passive tracer model (which transports the tracer, but it does not affect the oceanic circulation) with an active tracer model (in which temperature and salinity impact on ocean dynamics) (Foujols *et al.*, 2000). In the proposed ATM, the MLD is treated as a variable, but it is assumed that changes in the MLD are not large enough to cause a significant adjustment of the oceanic velocity field, which is determined by the wind stress and geostrophy. Above the MLD the salinity field was set up to respond to the atmospheric influences (E-P) plus advection

and entrainment determined from the hydrodynamic model, while below the MLD it is derived from the hydrodynamic model alone. The computation of the MLD uses the temperature from the hydrodynamic model; meanwhile, the salinity field is a response of the atmospheric effects on the upper layers of the ocean. This is a somewhat unusual concept, and its construction and development will need to pass rigorous justification.

The hydrodynamic model

The hydrodynamic model used in this study was the MOM, which is a three-dimensional, z-coordinate, B-grid, primitive equation ocean circulation model. The model was designed and developed by researchers at the Geophysical Fluid Dynamics Laboratory (GFDL/NOAA - Department of Commerce) as a numerical ocean modeling tool for use in studying ocean circulation over a wide range of space and time scales, which represents the state of the art in ocean modeling at GFDL near the end of 1999. The NOAA tropical Pacific Ocean primitive equation model employed here has been widely used in the study of equatorial ocean phenomena. It is part of the operational tropical ocean analysis project at the National Centers for Environmental Prediction (NCEP) (e.g., Ji & Leetmaa, 1997). Specifically, the MOM used in this study is its second version (MOM2), which was adapted by Dr. Gabriel Vecchi (NOAA/GFDL) and Dr. D. E. Harrisson (NOAA/PMEL), from previous versions of Philander *et al.* (e.g. Philander *et al.*, 1987; Philander & Seigel, 1985; Pacanowski & Philander, 1981). It can be found in greater detail in Vecchi & Harrisson (2003) and Harrisson *et al.* (2000).

Spatial and temporal features are presented as follows. Where changes have been made specifically for this study, they appear in parentheses.

Longitude: entire Pacific Ocean basin, with a resolution of one degree (for this study, from 145°W to the western American coast);

Latitude: from 12°S to 12°N, with a resolution of 1/3 degree;

Depth: from surface to 100m depth, with 10m resolution (which was addressed to better solve the oceanic mixing layer, the focus of this study), and from there spanning to 450 m. In total, the depth axis consists of 20 vertical levels; and,

Time: from January 1st 1986 to August 31st 2002, with results provided as 3 day averages.

Wind stress was computed using the Large & Pond (1981) drag coefficient, using 1986-2003 from the European Centre for Medium-range Weather Forecasts (ECMWF-ERA40 from the ECMWF Data Server), 12-hourly, 2.5° x 2.5° degrees of resolution (operational 10-meter wind analysis); surface heat flux is parametrized as described in Harrison (1991), computing Air Temperature based on the model Sea Surface Temperature (SST) and the historical (AIRT-SST) as a function of SST; and, the hindcast was begun after a 10 year spin up with climatology, when salinity was restored to annual mean conditions as in Levitus (1982) climatology using a 50-day restoring scale. The surface salinity flux was set to zero.

The mixed layer model

The atmospheric dataset used to calculate the input variable $(E - P)$ (evaporation minus precipitation), used as the atmospheric freshwater flux, was provided by the ECMWF-ERA40. The dataset was linearly interpolated to achieve the same spatial and temporal resolution as in the hydrodynamic ocean model, which was described above. Although the simplest method of interpolation, the linear interpolation nevertheless keeps constant the rate of change within a segment (and so can easily be controlled). Note that the salinity in the upper ocean (mixed layer) is conceived as a sum of horizontal advection, vertical entrainment at the bottom of the mixed layer (the Mixed Layer Depth - MLD) and atmospheric influences on the ocean surface (due to precipitation and evaporation). The surface freshwater flux is so prescribed.

This process can be expressed as an oceanic mass conservation equation split into two layers, as follows:

$$\frac{\partial S_k}{\partial t} = \begin{cases} -\nabla(\vec{v}.S_k) - \dfrac{\sum_{z(k)=surface}^{z(k)\equiv MLD} S_k}{h}(E-P) & \text{if } z(k) \leq h \\ \\ -\nabla(\vec{v}.S_k) & \text{if } z(k) \geq h \end{cases} \qquad (4.1)$$

where, S_k is the salinity of layer k; $z(k)$ is the depth related to the layer k; $\vec{v}$ is a three-dimensional velocity field; h is the mixed layer depth and, E and P are the evaporation and precipitation rates, respectively. All variables have their units expressed in the International System.

Density of water at the sea surface is typically 1027 kg/m^3. For simplification, physical oceanographers often quote only the last 2 digits of the density, a quantity they call *density anomaly* or $\sigma(S,T,p)$:

$$\sigma(S,T,p) = \rho(S,T,p) - 1000\text{kg/m}^3 \qquad (4.2)$$

here ρ, S, T, p refers to density, salinity, temperature, and pressure. $\sigma(S,T,p)$ is typically 27.00 kg/m^3. Here, however, we will follow common practice and use σ.

Thus, within this context, the mixed layer depth follows the definition of Kara *et al.* (2000a, b), where the reference temperature is changed by the absolute difference of ΔT = 0.5°C from the temperature at 10m beneath the SST and, consequently, a change in reference density is induced by the equation of state. Then,

$$\Delta\sigma_T = \sigma_T(S, T + \Delta T, p) - \sigma_T(S, T, p) \qquad (4.3)$$

where σ_T is the density as a function of temperature (T), S is salinity and, p is the

pressure (set to zero). Further details of the algorithm used to construct the MLD can be found in more detail in Kara *et al.* (2000a, b).

The Active Tracer Model

Because the oceanic mixed layer responds so rapidly to surface generated turbulence through wind-forced and buoyancy-forced processes, the surface mixed layer can often be modeled successfully using one-dimensional (vertical processes only) physics, therefore the model assumes a uniform "well mixed layer". However, it is considered to be the upper boundary layer of the ocean forced directly only by the atmosphere through the atmospheric flow of freshwater (as a prescribed variable), although, the surface stress of the wind is implicitly considered (through the numerical interactions towards a vertical average into the mixed layer). Then as a consequence, the model aims to consider both the input of the atmospheric flow of freshwater, and the wind shear, which causes the turbulence needed to mix the upper layer. This is represented by the vertical average in the defined upper layers. If the ocean is subjected to evaporation (where $E > P$), then the buoyancy decreases (and density increases). The evaporation increases the density of the upper surface layer, causing it to overturn (convect) and mix to a greater depth than it was mixed initially. In an opposite sense, freshwater gain ($P > E$) decreases the density of the upper surface layer, resulting in a more stably stratified profile; so that the final mixed layer becomes shallower than the initial mixed layer.

To summarise, consider that for every time step, the model merges the atmospheric input of freshwater to the upper ocean surface and in so doing adds or reduces buoyancy as appropriate. The model then proceeds to calculate a new depth for the mixed layer, in terms of "mixed", i.e. vertically averaged saline properties. The consequent physical processes are numerically addressed in the model by means of the vertically averaged salinity computation, and this is performed for every time step,

from the ocean surface to the bottom of the mixed layer. Consequently, for every time step and for every grid point, the model generates an adjusted mixed layer water column of uniform salinity from which the modified depth of the mixed layer is calculated in accordance with the atmospheric input at the surface. Below the mixed layer depth, in the more quiescent deeper ocean, the mass field (i.e. density profile) is maintained unchanged, since it is not directly influenced by the atmosphere. In this entire process the velocity and temperature fields follow Vecchi & Harrison (2003). Above the MLD, then, the model ensures that salinity responds realistically to atmospheric influences of $(E - P)$ type, together with entrainment and advection. In the computational process, the atmospheric input is calculated from the ECMWF-ERA40, while the salinity field and MLD, dependent upon atmospheric input of freshwater, resultant salinity, temperature and resultant buoyancy are renewed for each grid point and for every time step.

In retrospect, this initiative combines the characteristics of two model concepts: a hydrodynamic model on the one hand and a mixed layer model on the other. In the present context, the adopted model cannot claim to be a true tracer model, since its treatment of salinity has a prognostic role simultaneously providing changes in the depth of the mixed layer for each grid point and for each time step. Note also that the proposed numerical approach does not consider turbulence in its process, the oceanic mixing layer being vertically mixed. Neither does it consider changes in the velocity field as a consequence of the entire process - the velocity field is prescribed as output of the MOM2. For these reasons, the model is neither truly tracer nor truly prognostic; its thrust lays in a rather different direction, hence the denomination of "Active Tracer Model" (ATM). On the basis of the characteristics of the ATM here outlined, its validation will comprise both comparisons of model output with the *in situ* data, but also its skills will be applied to previously visited tasks so as to allow comparison with relevant published work.

Before proceeding with the validation, a quick reminder is timely as follows: as defined in Part I, Response of the Ocean (Page14), the "Control Run" (Ctrl) is the ATM (and its output) given that the atmospheric flux of freshwater is based on $(E-P)$ with initial parameters being derived from their original source (the ECMWF-ERA40 dataset), but interpolated to achieve the spatial and the temporal resolution defined in this study. With this in mind, the next section will present the validation of the "Control Run" (Ctrl).

a) Validation of the "Control Run"

The time series analysis

In this study the main oceanographic parameter to retain focus throughout Part I has been salinity modification as a response to atmospheric forcing. Consequently, the presentation of the validation of the model will start with this variable and in its simplest form, namely by a comparison with observed time series. The comparison between the Sea Surface Salinity (SSS) as output by the Ctrl and *in situ* data provided by moored buoys from TAO program is shown in the Figure 4.1.
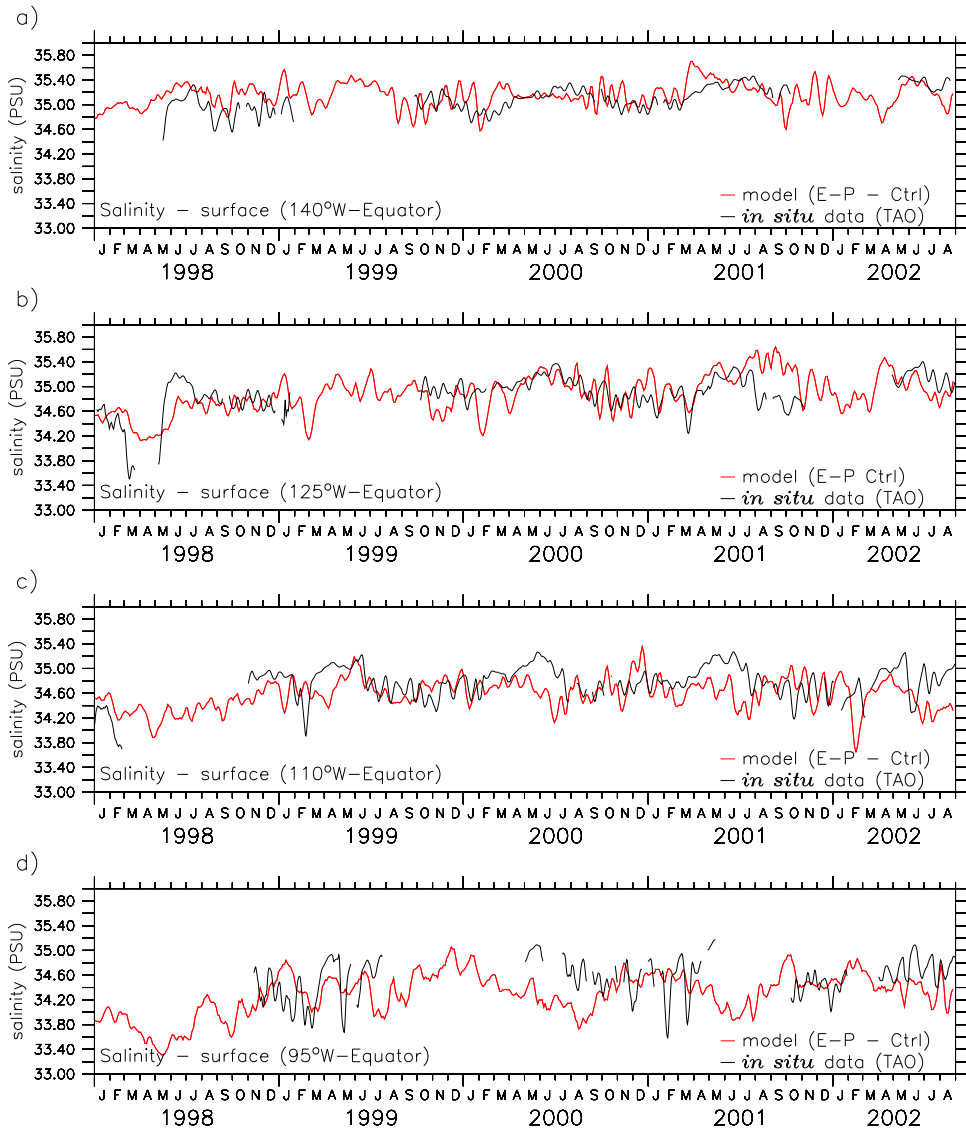
Figure 4.1: Time series of the Sea Surface Salinity (SSS) along the Equator, for longitudes 140°W (a), 125°W (b), 110°W (c) and 95°W (d), from the numerical model (Ctrl - red line) and *in situ* data from TAO moored buoys (black line).

At first glance, a comparison between the model (Ctrl) output and the observed data from the TAO program has its shortcomings as the relative time series of Figure 4.1. In Tomczak (1995), it is described that a single and localized heavy rain produces a shallow lens of freshened water, but the reduction in salinity can be so strong that the cooling associated with the atmospheric freshwater input (rainfall) can not be sufficient to initiate convection. Therefore, the work demonstrates the difficulties in establishing the salinity field in the upper layers of the tropical oceans. However this is considered to be a very demanding and stringent test and explained by the large spatial variability, and even on intensity of the tropical rain which creates difficulties in the practice of comparing actual point measurements from the sparse array of moored buoys with the concept of a grid-based model and its computational reproduction. Although the model did not predict accurately the magnitude of the salinity signal present in the higher frequencies, as can be seen from Figure 4.1, it is still worthy of note that the model in most cases did show sensitivity to higher frequencies. In this aspect alone, the model, overall, shows promise. Specifically seasonal and annual trends are well-produced. Consequently when used so as to take advantage of its skills in the longer time scales, it can assume the role of a tool quite complementary to established conventional approaches.

Secondly the question might be posed as to the general characteristics demonstrated by the Ctrl to maintain a realistic, but also sustained, level of output over the period of the tests. In this context, the long-term evolution of the salinity field as output by the Ctrl was investigated by the three-dimensional integration over the entire model domain volume (Figure 4.2).
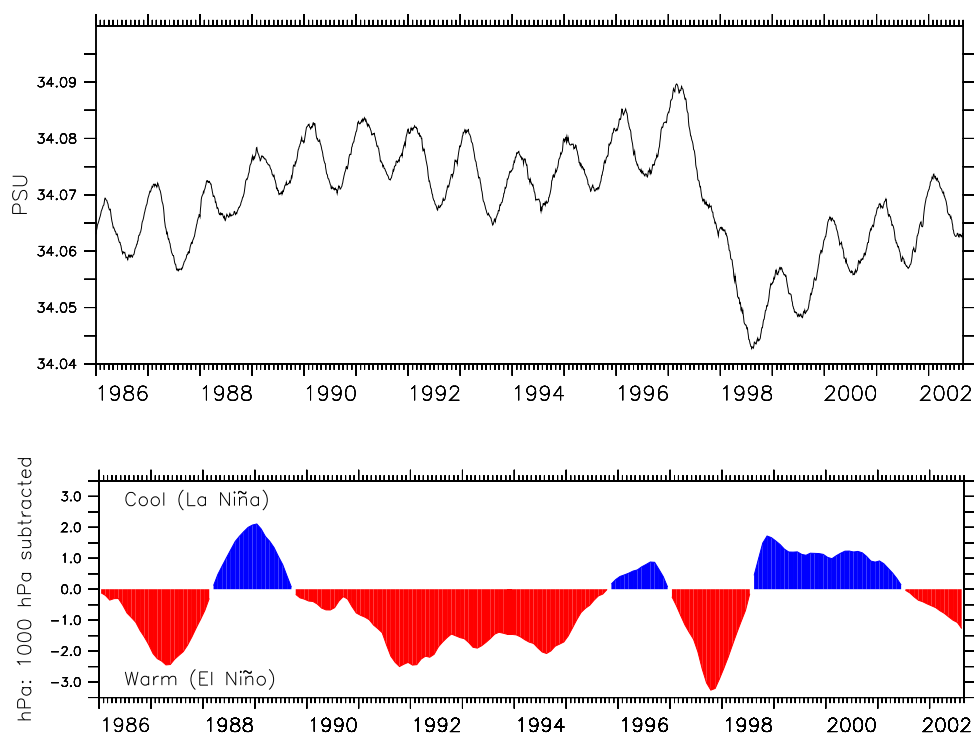
Figure 4.2: **Upper panel:** Time series of salinity field volume-integrated (as output of the Ctrl) over the entire model domain. **Lower panel:** Southern Oscillation Index (SOI) based on the Trenberth method - monthly standard deviation and one year smoothed. SOI unit: hPa (1000 hPa subtracted).

What is significant in terms of confirmation of the integrity of the model is the longer term signal seen in the integrated salinity upon which is superimposed a regular and expected annual cycle. The presence of both signals in the model output is welcome but especially welcome is the fact that the background long term trends of the integrated salinity are clearly associated with the timescale of the multi-year decadal variations of the SOI. However, the enhancement of the integrated salinity variability over the entire period must not be seen as a direct response to the SOI, but as an outcome of the non linearity of the ENSO effects (Hoerling *et al.*, 1997). With regard to the non-linearity response to the features of the El Niño, in McPhaden (1999) there is presented a study explaining how during the last strong El Niño an energetic Madden

Julian Oscillation (MJO) variation contributed to an unexpectedly rapid SST warming in early 1997 and a sudden cooling in mid-1998 in the equatorial Pacific. The MJO is an atmospheric feature characterized by an eastward progression of large regions of both enhanced and suppressed tropical rainfall, observed mainly over the Indian Ocean and Pacific Ocean. The anomalous rainfall is usually first evident over the western Indian Ocean, and remains evident as it propagates over the very warm ocean waters of the western and central tropical Pacific. This pattern of tropical rainfall then generally becomes very nondescript as a localized tropical 40-50 day periodicity in winds and precipitation can be generated outside of the equatorial waveguide through coupled interactions among convection, the large-scale circulation, and the oceanic mixed layer (e.g. Madden & Julian, 1971, 1972; Maloney & Esbensen, 2003; Bielli & Hartmann, 2004; Maloney & Sobel, 2004).

Furthermore, the intensity of the effects of the ENSO cycle is related to the oceanic conditions of the preceding months. There remain several contesting hypotheses as to why the independent components of the ENSO cycle seem to interact, one with another, in a non-linear fashion. One may note for example that in the sustained El Niño period of 1990-1995, the volumetric integrated salinity did not display a strong reaction similar to those induced by the more temporally restricted episodic events of 1986/87 and 1997/98.

The SSS was selected as the first target variable and a natural prime indicator for the response of the eastern tropical Pacific to the variability of atmospheric freshwater reaching the region, and it has been noted that its role has been seen to have been replicated, at least partially, by the model. Nevertheless, a strong case was argued earlier for the "hybrid" nature of the model, in that it was designed to incorporate the processes active in the mixed layer and in particular the variability in depth of the mixed layer. It is this aspect of the Ctrl to which the verification of the model now turns.

The MLD is a derived variable calculated from the salinity, temperature and pressure of the oceanic fields arising from the equation of state of the seawater. With this in mind, the intention is to show the reliability of these two important parameters (salinity and temperature) as output by the model, given the pressure was set to zero.

In this context, the choice made is to show the depth of the 20°C isotherm (Z20) as output by the model and for the duration of its run. The Z20 time series has a dual significance in terms of the validation, firstly, because it shows the skill of the model in relation to the reproduction of the temperature itself and, secondly, at the same time, checks the sensitivity of the model in relation to its vertical incursion. The Figure 4.3 shows the time series of the Z20 along the Equator for the following longitudes 140°W, 125°W, 110°W and 95°W, as output by the numerical model (Ctrl), and also by *in situ* data from the TAO array.
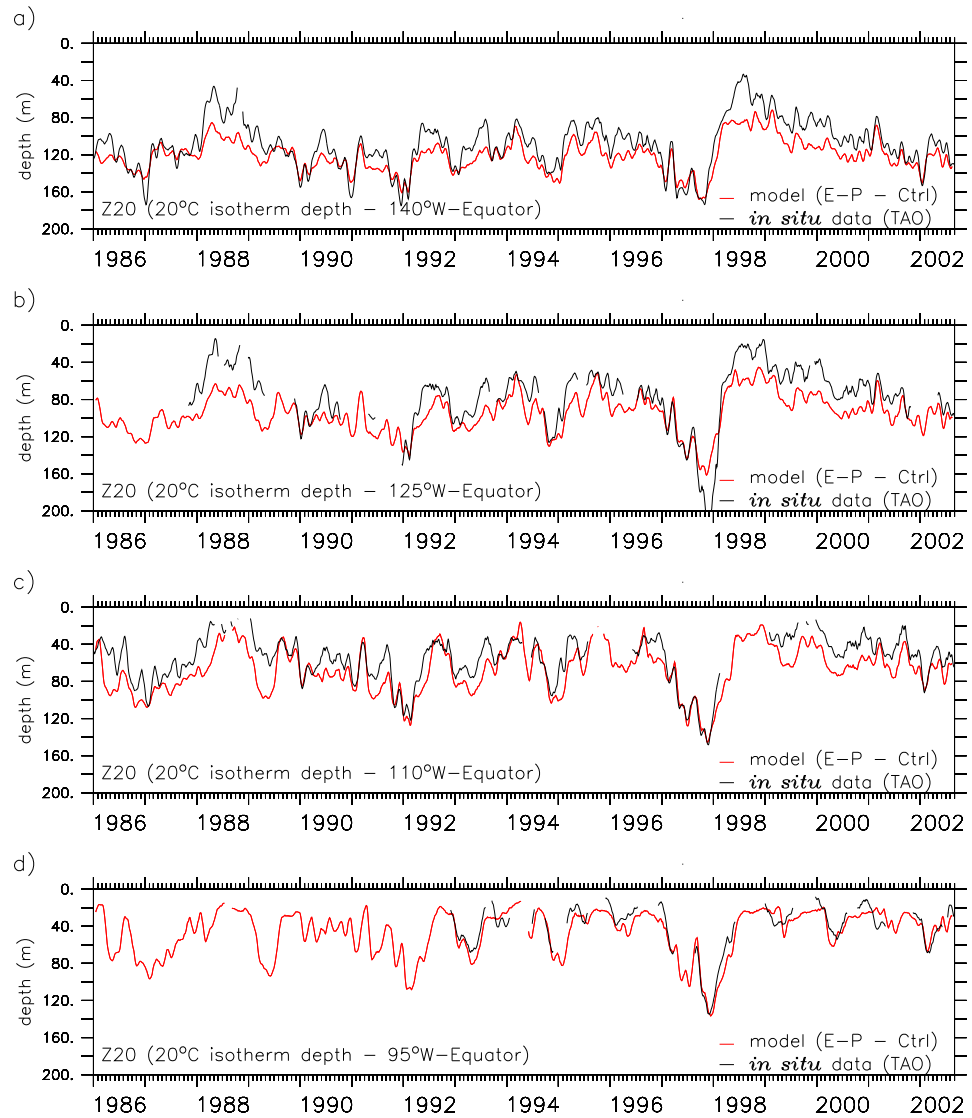
Figure 4.3: Time series of the depth (m) of 20°C isotherm (Z20) along the Equator, for longitudes 140°W (a), 125°W (b), 110°W (c) and 95°W (d), from the numerical model (Ctrl - red line) and *in situ* data from TAO moored buoys (black line).

The depths of the 20°C isotherm (Z20) along the Equator are well represented in output of the model when compared with the *in situ* data provided by moored buoys from the TAO program, in the low and the high frequencies (Figure 4.3).

Up to this stage the validation procedure has been based upon direct comparisons between output from the Ctrl and actual measured data. The aim now is to advance the validation to an analytical phase whereby Ctrl output is first subjected to analysis and the analytical results compared with the findings of other published scientific work.

Meanwhile it should be noted that the success of the validation to date has a bearing upon the credence to be allocated to the preliminary use of the Ctrl in Part I where model runs were applied to various data series of atmospheric-sourced parameters. This belated confirmation of the model output resulting from similar applications to observed data lends confidence to those earlier findings.

The time-space variability of the SSS

Returning to the Ctrl validation in its second analytical phase, the attention is again initially given to salinity. The Empirical Orthogonal Function (EOF) was used to determine the time-space variability of the Sea Surface Salinity (SSS), and the results of this statistical technique for its first three modes when applied to the monthly mean of the SSS are shown in Table 4.1.

Table 4.1: Results for the first three EOF modes when applied to the monthly mean of Sea Surface Salinity (SSS) as output by the Ctrl.

EOF mode	SSS variance (%)
1	35
2	13
3	6

The Figures 4.4, 4.5 and 4.6 present in their upper panels the spatial patterns of the three leading EOF modes, respectively to the first, second and third modes. The lower panels of the same figures display the respective temporal variation of expansion coefficients of the same first three modes of SSS.
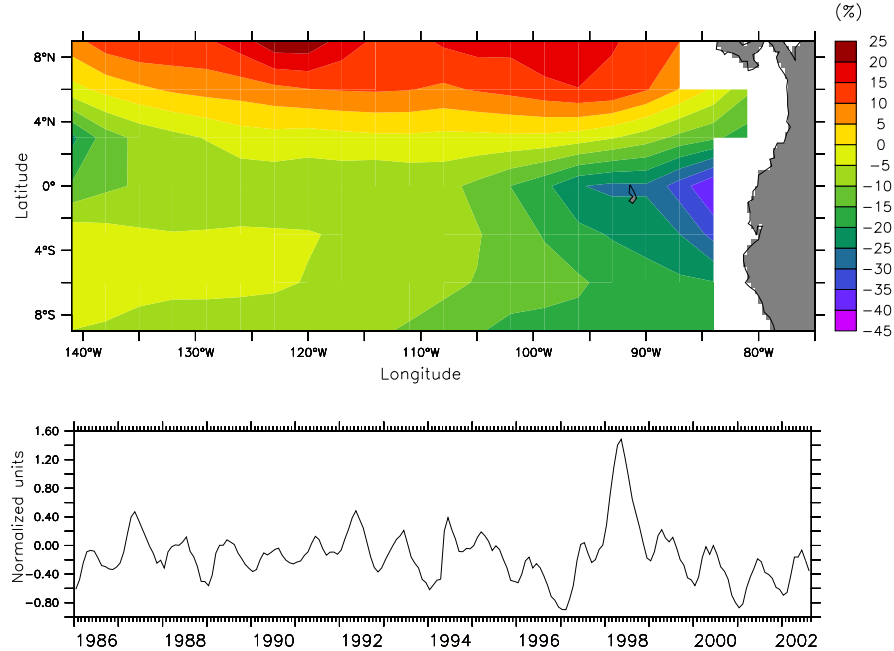
Figure 4.4: **Upper panel**: Spatial pattern of the first EOF mode of the monthly mean of the SSS (which accounts for 35% of the total variance) is presented as the spatial distribution of the percentage of variance accounted for the first mode. **Lower panel**: Time series of the expansion coefficients of the first EOF mode of the monthly mean of the SSS (in normalized units).
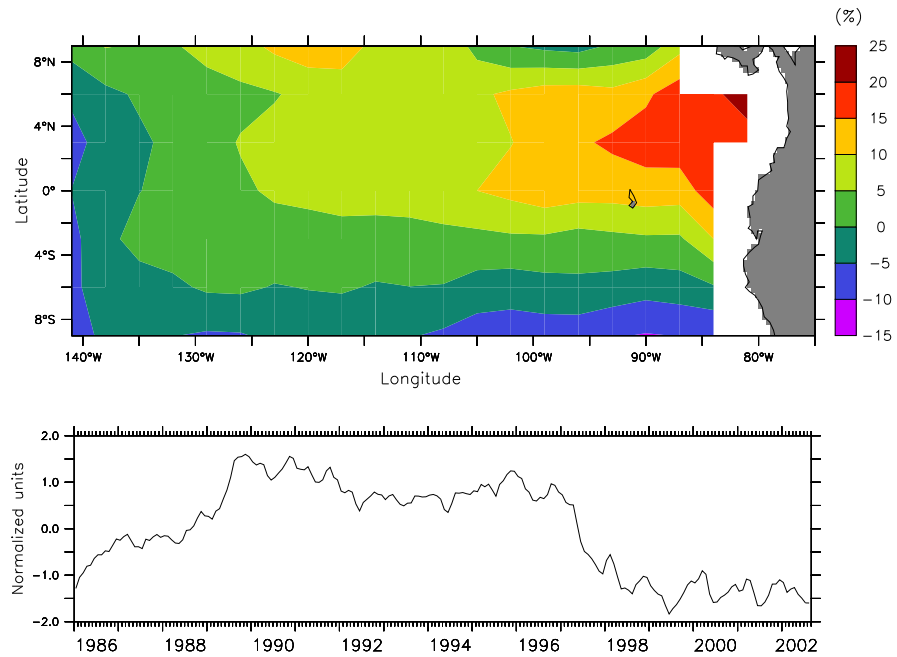
Figure 4.5: Same as Figure 4.4 but for the second EOF mode of the SSS (which accounts for 13% of the total variance)
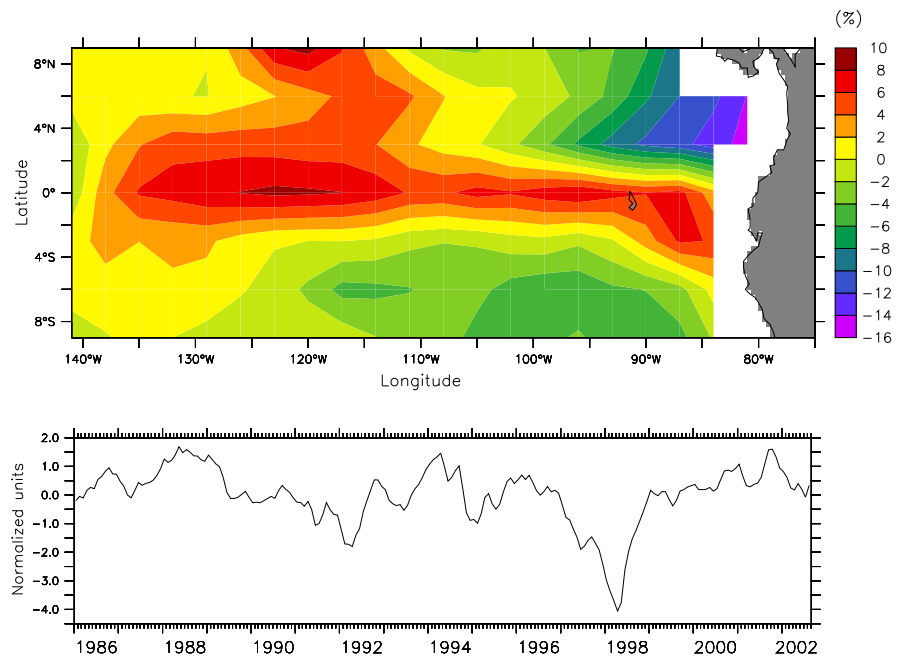

Figure 4.6: Same as Figure 4.4 but for the third EOF mode of the SSS (which accounts for 6% of the total variance)

The resultant features of the EOF analyses when applied for the monthly mean of the SSS, both the spatial pattern and the associated time series, are in good agreement with the study carried out by Delcroix *et al.* (1996), who worked on "ship-of-opportunity" water sample measurements made in the tropical Pacific region for the 1974-1989 period. Their data had been spatially interpolated and monthly-averaged before being subjected to statistical analysis. The most evident result in both studies, the present one and that one carried out by Delcroix *et al.*, is that the eastern Pacific Ocean basin separates into two regions (Figure 4.4 - upper panel), where the dividing line is the mean positioning of the ITCZ (about 5°N), while the time series associated with the spatial pattern of the first EOF mode reproduced the seasonal and ENSO scales. Later, in 1998, the same author (Delcroix, 1998), from an extended basis of data in relation to his previous study, performed statistical analyses and confirmed the patterns above described, despite that, in this latter study, the objectives were broadened to include the inter-comparisons of the SSS, SST, precipitation, wind stress and dynamic height.

The work of relevant authors in this field has seen significant escalation partly based upon increasing data quality, but also in the techniques employed. A consequent growing confidence has seen an expansion in the challenges accepted. Comparisons with such work will be provided later, consequent upon further progress with the treatment of time-space variability of the SSS.

At this point, despite the good agreement of the present work with previous published work (Delcroix *et al.*, 1996; and Delcroix, 1998), it is important to focus attention upon each of the associated time series, which present an evident non-periodic pattern. The intention now is to re-examine such signals (the lower panels of Figures 4.4, 4.5 and 4.6) with respect to their own time-frequency dependencies.

The foregoing study of the time-space variability of the SSS has had as its goal a direct assessment of the analytical analysis of the EOF in relation to relevant work by other authors and in so doing strives to gain confidence in the validity of the model. The opportunity now arises to introduce an additional inquiry into the characteristics of the time variability itself which offers the promise of acquiring a better understanding of the characterization of the SSS as a whole. In this way the intention is to temporarily step outside the initial task of validation of the model. With such an approach, not only could the lead be given to a contribution to a broadening of the frame of associated knowledge, but also will provide its own support to the general discussion of regional time-space variability of the SSS in the eastern Tropical Pacific, not least being the needs of the current study as it evolves into a growing comprehension of the SSS. This digression will address the time series of the expansion coefficients derived from the EOF as applied to the monthly mean of the SSS as an opportunistic and innovative procedure triggered by the current study and not as an essential step in the model validation process itself.

In this context, the use of the Wavelet technique seems to be a valuable tool to reveal such aspects of the time dependence of those signals, because the EOF analysis considers the time series as a standing oscillation signal, and not propagating patterns as wavelet analysis does; moreover, it is worthy of note that an approach of this type was successfully employed in a similar sense in Part I of this study. Then, with the intention to expand knowledge of the SSS in the time variability basis in mind, the Wavelet technique was applied to the time series of the expansion coefficients derived from the EOF applied to the monthly mean time series of the SSS. Again Morlet ($\omega_0 = 6$) was adopted as the mother wavelet, and the results of this approach are given in the Figures 4.7, 4.8 and 4.9, respectively for the first, second and third EOF leading modes.
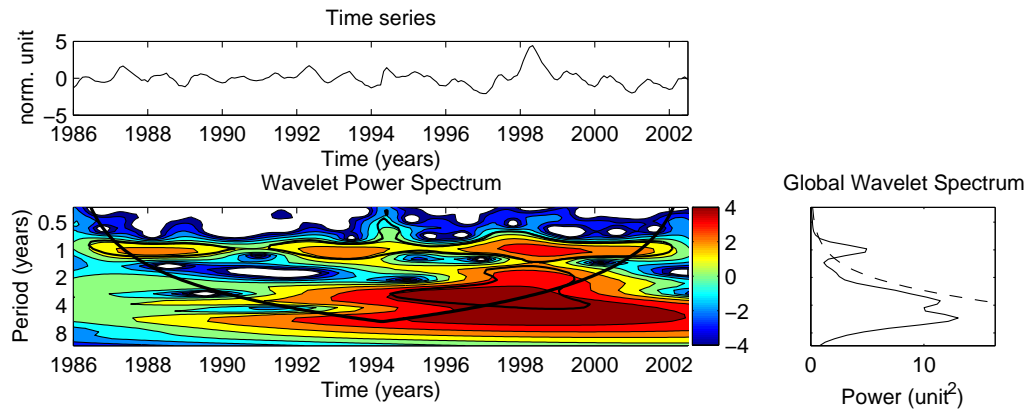
Figure 4.7: Results of Wavelet analysis for the expansion coefficients of the first EOF mode of the SSS. The time series is plotted in the top diagram, the contours of the Wavelet power spectrum (middle panel), and the global Wavelet power spectrum (right panel). The dashed line in the right panel represents the confidence level of 95%. The contour Wavelet power spectrum levels are chosen so that 75%, 50%, 25%, and 5% of the wavelet power is above each level, respectively. The dark line indicates the cone of influence (COI). "COI is the region of the wavelet spectrum in which edge effects become important" (Torrence & Compo, 1998)
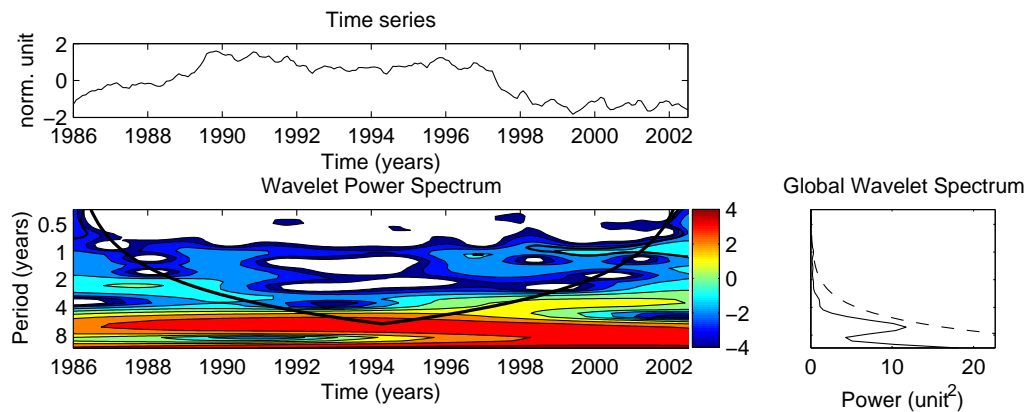

Figure 4.8: Same as Figure 4.7 but for the expansion coefficients of the second EOF mode of the SSS
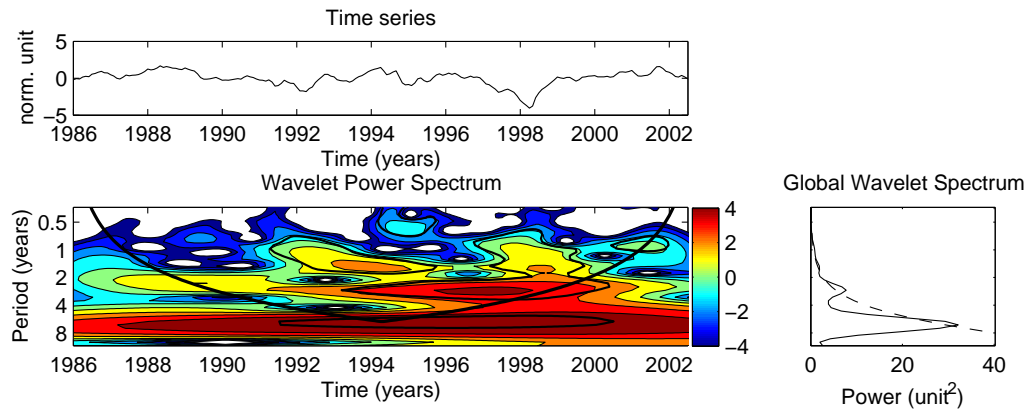
Figure 4.9: Same as Figure 4.7 but for the expansion coefficients of the third EOF mode of the SSS

The application of the wavelet decomposition technique has greater power than is called upon here. For example, when the wavelet technique was applied to the time series of the expansion coefficient of the first EOF mode, its wavelet power spectrum gives evidence of one remarkable characteristic (Figure 4.7 - middle panel) which is not perceptible by the visual inspection of the expansion coefficients of the first EOF mode of the SSS (also reproduced Figure 4.7, in its top panel): the interruption to the signal referring to one year period. Similar conditions are also observed in the analyses carried out by the wavelet technique for the second and third time series associated with respective leading EOF modes (Figure 4.8 and 4.9, respectively). The validation phase focusing on the time-space variability of the SSS was deemed to have achieved its purpose through the use of the EOF technique as previously presented. However, in the process of applying the Wavelet technique to the time-series of the respective EOF modes which followed, there emerged indications that by combining the two processes (EOF and Wavelet) it might be possible to examine significant aspects of their combination as yet unidentified. While not wishing to distract attention from the process of model validation at this juncture, yet attracted to the potential of this argument, it was concluded to defer attention to a later section.

Consequently, discussion returns to the model validation procedure and in this context the focus switches to a comparison of certain aspects of the Ctrl output with relevant features of previously published works. Validation may take many forms, but the prime focus here is to verify the consistency of the output of the present model when compared with published analyses based upon observational data and in this manner to confirm and refine the earlier validation procedures applied to the Model.

The zonal fields along the Equator

The attention now turns to the performance of the model in its treatment of ocean currents confined in the domain of the study through a comparison of its achievement with previously published works. Johnson *et al.* (2002b) describe the zonal velocity in the upper layer of the Pacific Ocean using synoptic, meridional and zonal sections obtained by CTD/ADCP, mostly conducted in the 1990's. The option here is to present sections of the mean fields along the Equator for zonal velocity, temperature and salinity. This choice was based on the opportunity to present simultaneously some features that are, in a general sense, characteristic of the region. For example, firstly, in relation to the zonal currents along the equatorial region, the eastern-most region of the equatorial Pacific is targeted where the Equatorial Under Current (EUC) terminates; secondly, the vertical distribution of the salinity, which presents the lower surface values in the coastal region of Central America, and higher salinity values somewhat associated with the EUC; and finally, the vertical distribution of the temperature throughout the Equator, which presents inclined isotherms, leading to a shallower gathering of isotherms in the eastern basin, while it presents a vertical displacement of them towards the date line. Thus, the isotherms present a negative slope from the eastern to the western domain of this study. The Figure 4.10 displays sections of the mean fields for zonal velocity, salinity and temperature along the Equator as estimated by the Ctrl output.
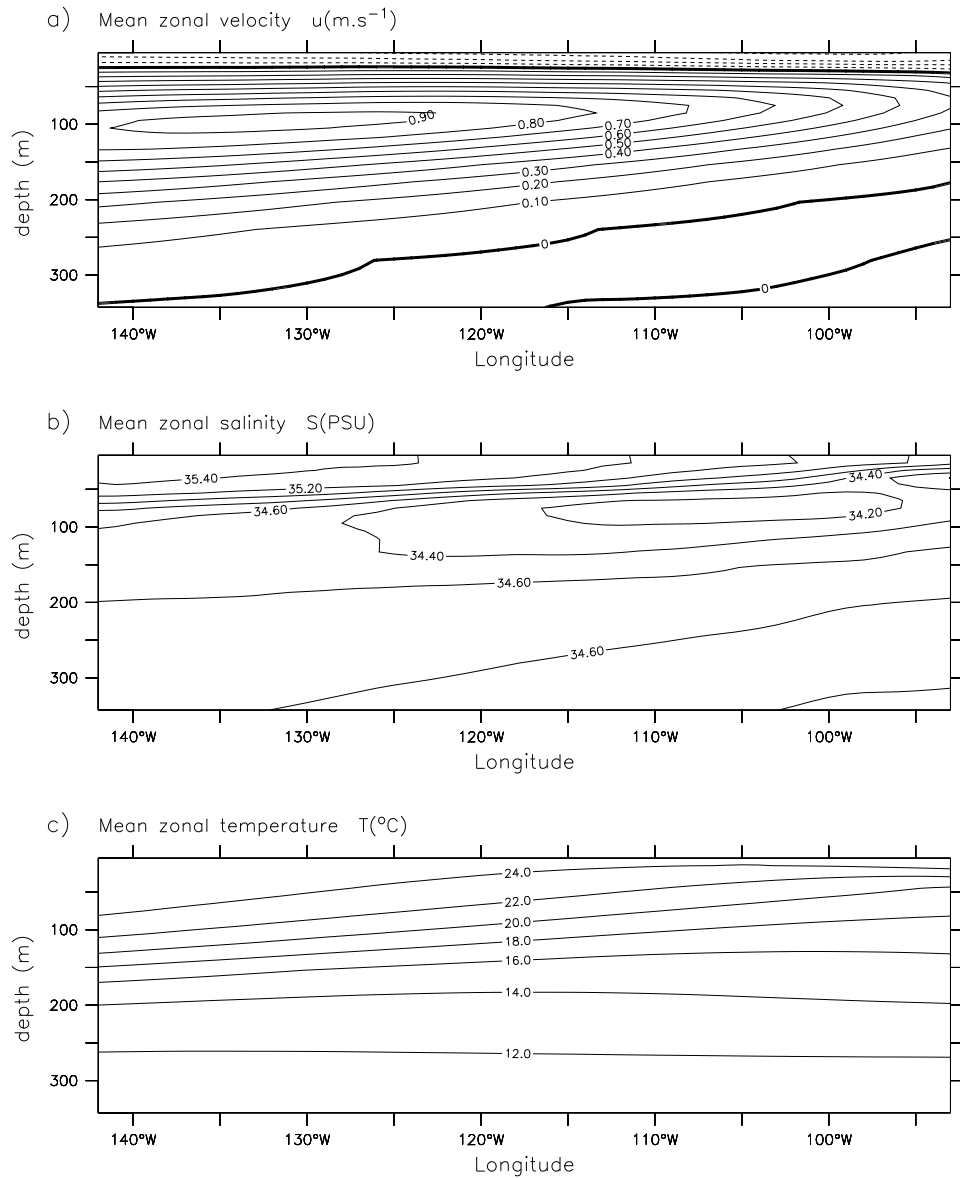
Figure 4.10: Sections of the mean zonal fields along the Equator as estimated by the Ctrl output. (a) Mean zonal velocity (m/s). The contour interval is 0.1 m/s, and solid lines represent eastward flow, dashed line represent westward flow and thick line the null zonal velocity. (b) Mean zonal salinity (PSU). The contour interval is 0.2 PSU. (c) Mean zonal temperature (°C). The contour interval is 2°C.

The spatial termination of the EUC was described via upwelling processes in the observational study of Lukas (1986) as occurring in the eastern region between the Galapagos Archipelago (the Galapagos islands are centered at 0°, 91°W) and 5°S. Then Pedlosky (1988), using a theoretical model, suggested that the termination of EUC may be regarded as an inertial jet. The study of Sloyan *et al.* (2003) suggested that both mechanisms are relevant in the EUC termination. In the present work, the upper panel of the Figure 4.10 displays the isolines of the mean zonal velocity estimated from the Ctrl from which an eastward deceleration is suggested together with an upward motion of the EUC (note the tilt of the base of the isolines of velocity). Both features suggest that the EUC termination is well represented in the numerical approach of the current study. With regard to the mean zonal distribution of the salinity field (Figure 4.10 - middle panel), this presents an eastward decrease of magnitude on the surface, which may be interpreted as consistency with the fact that precipitation in the eastern tropical Pacific is the genesis of the zonal gradient of surface salinity. Finally, the lower panel of the Figure 4.10 presents the zonal mean temperature field output from the Ctrl run of the model. The observed eastward gradient of the isotherms in the lower panel of Figure 4.10 is coupled with upwelling from the EUC through the upper ocean layers. The gradient of the isotherms gives to the easternmost region the minimum sea surface temperature of the equatorial Pacific Ocean. The panels representing the mean zonal fields along the Equator confirm the expected patterns, and furthermore, they are in a good agreement with the results presented by Sloyan *et al.* (2003), which used the same set of observational data earlier used by Johnson *et al.* (2002b).

The volume transport by the eastern equatorial current system of the Pacific Ocean

Despite the good agreement achieved, the results presented for the section along the Equator have the inconvenience of providing only a snapshot of those parameters; consequently, it is intended to develop an additional investigation with particular reference to time evolution of the hydrodynamics of the model. In this context, the

implications for volume transport within the confines of the domain of the study are investigated. The current boundaries will follow the definitions of Johnson *et al.* (2002b), their criteria being: potential density, main direction and geographical position, as set out in Table 4.2. The potential density (σ_θ), as one of the defining parameters of the oceanic currents, is the density a parcel of water would have if it were raised adiabatically to the surface without change in salinity. Thus, the intention is now to transpose the validation procedure to the volume transport of the main currents of the eastern equatorial Pacific as one method of evaluation of the hydrodynamic functioning of the oceanic model.

Table 4.2: The eastern equatorial Pacific Ocean current system's definition (Johnson *et al.*, 2002b). Equatorial Under Current (EUC). North Equatorial Counter Current (NECC). South Equatorial Current - North branch (SEC(N)). South Equatorial Current - South branch (SEC(S)). The potential density (σ_θ) is the density of a parcel of water would have if it were raised adiabatically to the surface without change in salinity.

Current	Potential density interval (kg.m^{-3})	Latitude interval	Direction
EUC	$23.0 < \sigma_\theta < 26.5$	$2°S < Lat < 2°N$	eastward
NECC	$\sigma_\theta < 26.0$	North of 2°N	eastward
SEC(N)	$\sigma_\theta < 26.0$	$0°N < Lat < NECC$	westward
SEC(S)	$\sigma_\theta < 26.0$	$8°S < Lat < 0°N$	westward

The volume transport as output from the Ctrl with regard to SEC(N), EUC and SEC(S), according to definitions in Table 4.2, is shown in the Figure 4.11, and as the model domain did not extend sufficiently far north, then, the NECC was not included. Kessler *et al.* (2003) carried out a similar approach with the domain of volume transport integration slightly different from material presented in the Table 4.2. In their study, they used a generalized definition of the domain, where there are no density restrictions, the domain being defined only by the main direction and geographical position of the currents. In Kessler *et al.* (2003), the current definitions are as follows: for

the SEC(N), the westward transport between the Equator and 5°N; for the EUC, the eastward transport between 3°S and 2°N; and for the SEC(S), the westward transport between 8°S and 2°S. Moreover, the study was based on three methods: a) the Sverdrup circulation of the tropical Pacific using scatterometer winds, b) measured ocean currents, and c) diagnosis by an oceanic General Circulation Model (GCM). Kessler *et al.* present the integrated zonal volume transport for each one of their methods of computation: carried out by the Sverdrup balance, by current measurements using ADCP and by the output of numerical modeling. Meanwhile, the results achieved by the present study in relation to the zonal current volume transport for SEC(N), EUC and SEC(S) are presented in the Figure 4.11.
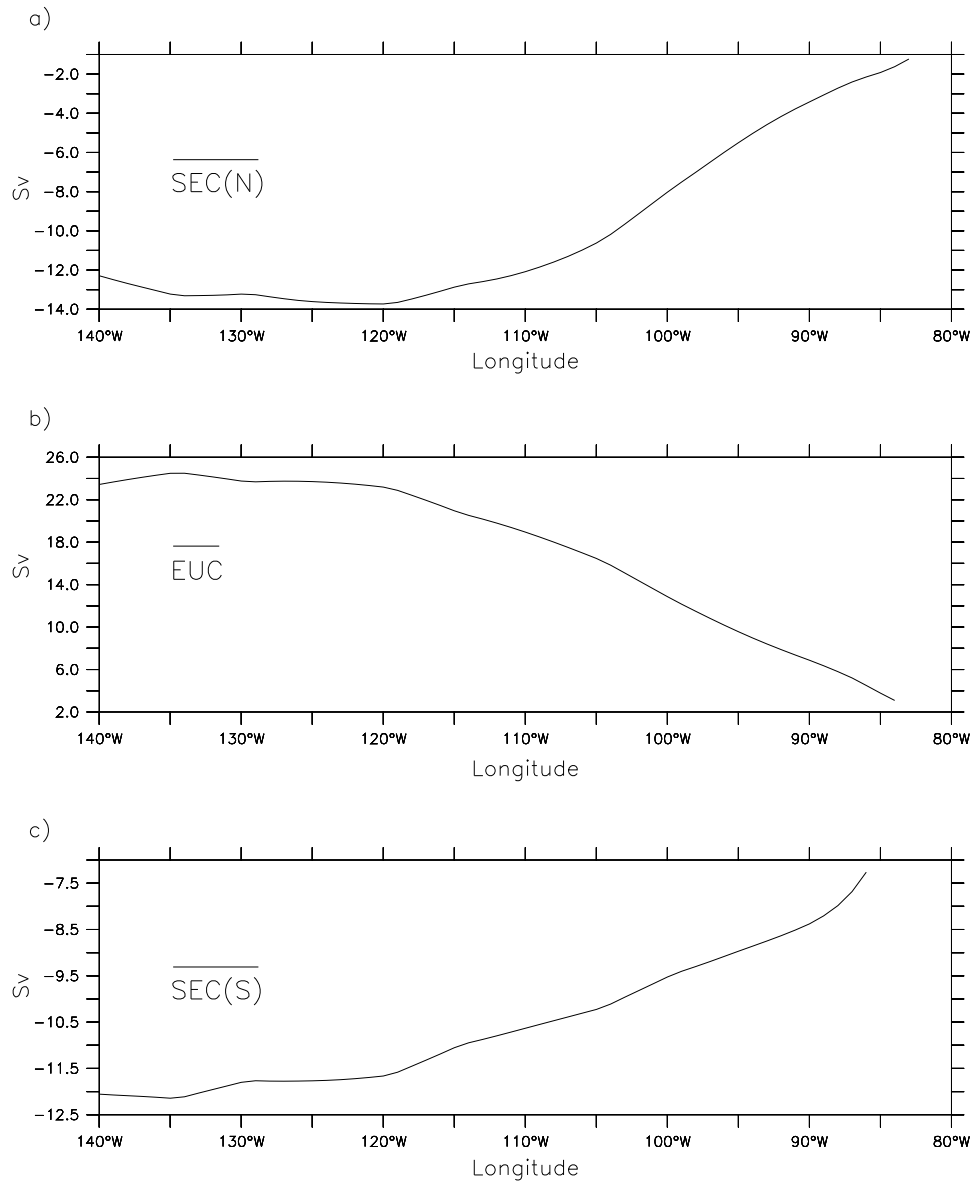
Figure 4.11: Time-vertical-meridional average of the zonal current volume transport, as output from the Ctrl, for SEC(N) (a), EUC (b), and SEC(S) (c) in the eastern equatorial Pacific Ocean. It adopts the current definitions by Johnson *et al.* (2002b), which are summarized in the Table 4.2. The vertical scale is different for each current system (Sv = 10^6 m^3.s^{-1}). Eastward volume transport is represented as positive.

In the analysis of the results achieved by the current work, it is possible to observe the reduction of the volume transported by the EUC (Figure 4.11 - middle panel), as a direct consequence of the termination of EUC in the eastern Pacific, as previously presented here in the analysis of the time-averaged zonal velocity section along the Equator (Figure 4.10 - upper panel). In an analogous manner, from the observation of the zonal volume transport associated with the two westward currents (SEC(N) and SEC(S), the upper and lower panels in the Figure 4.11, respectively), it is possible to note the zonal increasing of the volume transport associated with them. In particular, they change negatively according to their displacement westwards from the eastern boundary of the domain. Although reference has already been made to the fact that slight differences have been noted in the definition of current boundaries in both studies, and again in the work of Kessler *et al.* (2003) with consequent concerns as to the zonal volume transport achieved, nevertheless a significant degree of conformity exists.

The salinity field associated with the eastern equatorial current system of the Pacific Ocean

Both Johnson *et al.* (2002b) and Kessler *et al.* (2003) had conducted hydrodynamic studies of the Pacific Ocean; however, when they had the availability of data, associations with the salinity field had also been made. In a similar manner, wherever possible, links between current fields and salinity fields will therefore be pursued using the output from the Ctrl. The intention will be to enrich the validation of the oceanic model, or to extend the characterization of the salinity field where such information is lacking. This practice then offers a twofold function: both as a possible validation of the model on the one hand and also as a supplement to the findings of Johnson *et al.* and Kessler *et al.* on the other.

It is accepted that, the definition for the equatorial current of the Pacific Ocean described in the Table 4.2 confines a finite and volumetric region of the ocean, which is dynamically adapted to the temporal and spatial variability of the currents, in accordance with the dynamic variation of the parameters that define them. Thus, such regions, individually associated with the respective current, at the same time are associated with the specific bodies of seawater which are related to the current. This dual role may serve to provide a volume controller to the salinity field, and simultaneously a temporal-spatial association with currents.

A limitation of the foregoing approach lies in the fact that very little information about the salinity field linked to the currents in the eastern Pacific Ocean was found in the literature, which makes comparative studies somewhat limited in the validation context, but the same limitation implies that valuable new information may be expected to be obtained by progress in this area. In summary, on the one hand, there is a limitation imposed referring to the validation process, but on the other, there exists the intention to extend knowledge in relation to the salinity field associated with the currents in the eastern tropical Pacific.

With this in mind, it is now proposed to address salinity associated with the equatorial current system of the eastern Pacific Ocean by a comparison of the Ctrl run of the model in this respect with previously published work. Given the paucity of the latter and the consequent limits to the approach, this reference will be to that carried out by Johnson *et al.* (2002b), based upon CTD/ADCP measurements and described earlier in this section. In this context, the output of the Ctrl in terms of the zonal time-averaged mean salinity associated with the equatorial current system of the Pacific, as defined in Table 4.2, is presented in the Figure 4.12.

a)

Mean zonal salinity (PSU) associated with SEC(N)

b)

Mean zonal salinity (PSU) associated with EUC

c)

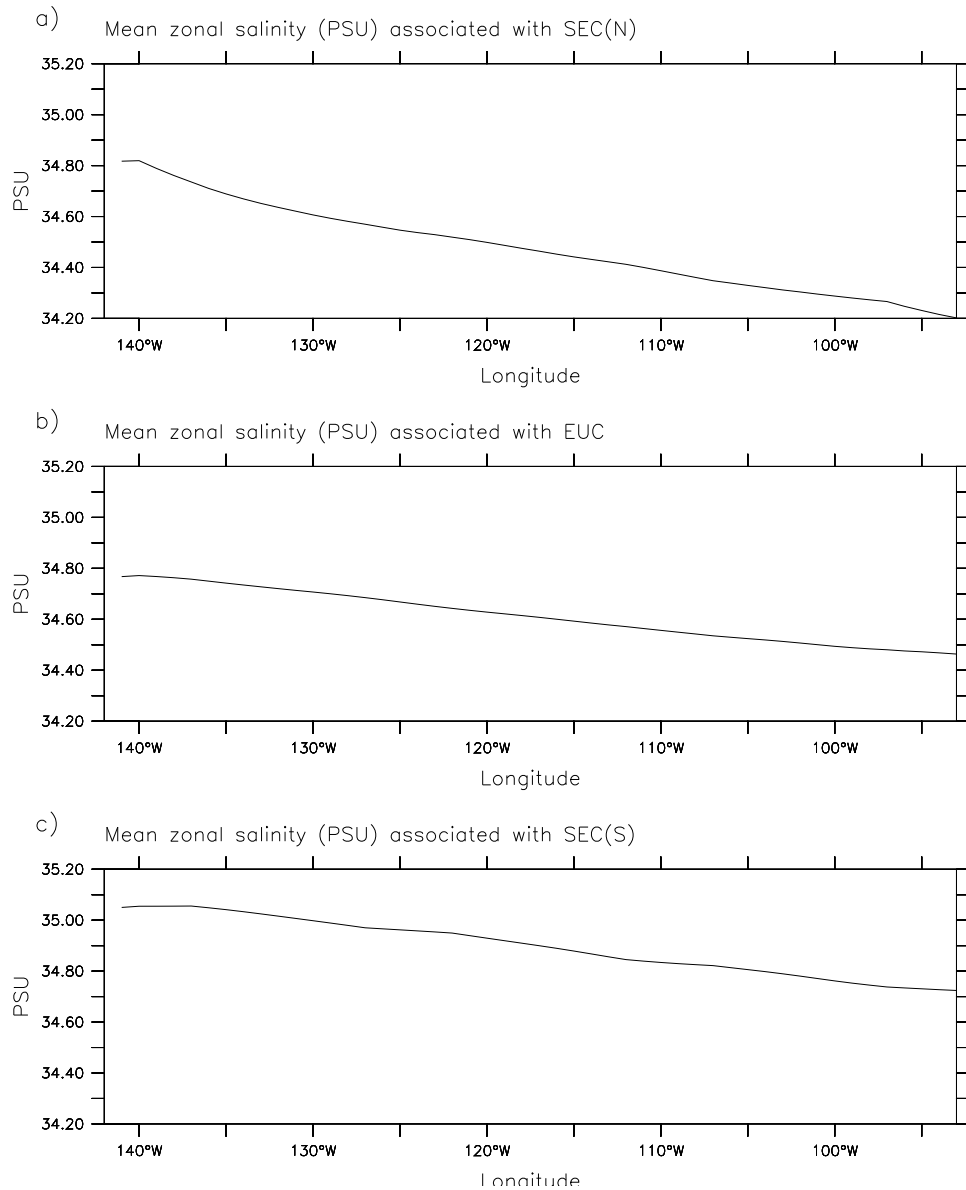Mean zonal salinity (PSU) associated with SEC(S)

Figure 4.12: The time-averaged mean salinity field (PSU) associated with the equatorial current system of the eastern Pacific Ocean as output from the Ctrl. The time-averaged salinity field (PSU) associated with the SEC(N) is shown in the upper panel (a), when associated with the EUC is shown in the middle panel (b), and the salinity field associated with SEC(S) in the lower panel (c). The vertical scale is the same for all panels to facilitate comparisons among them.

Regardless of the fact that the study carried out by Johnson *et al.* covered the entire Pacific Ocean basin throughout 10 zonal sections of CTD/ADCP measurements, the analysis here is limited to east Pacific Ocean basin as defined by the domain of the present study. Comparisons between model output and these observations for the time-averaged salinity associated with the equatorial currents in the eastern Pacific individually for SEC(N) and SEC(S) can claim to be in excellent agreement, with computed values differing from those of Johnson *et al.* based upon measurements, by 0.05 PSU and 0.1 PSU respectively. Concerning the EUC, the present study underestimated the salinity by about 0.05 PSU (at 95°W), with a westward linear increase to reach 0.3 PSU (at 140°W) when compared with that carried out by Johnson *et al.*. Even so the present study and that carried out by Johnson *et al.*, present the zonal time-averaged mean salinity with a trend of increasing values of salinity from the easternmost Pacific towards the date line, for each of the three currents being examined in the analysis.

The latter feature might well be a common characteristic of the salinity associated with such currents and therefore peculiar to this particular region. Given the knowledge available it is inevitable that it is assumed to provide a measure of corroboration of the influence imposed on the salinity of the region by the local precipitation, and so irrespective of current direction (*see* Table 4.2) their lowest salinities are to be found in the eastern equatorial Pacific. This is to suggest that it is possible to assume that the time-space variability of the precipitation studied in Part I of this study might, in some manner, reproduce its signature in the salinity associated with the currents.

In an attempt to clarify such matters, further and more intensive studies are contemplated in connection with the association of salinity properties with current systems. There is of course a limitation to be faced due to the paucity of *in situ* data, thus, the validation procedure will rely on published material on the subject to make comparative checks on model validity being sufficiently realistic. Having noted the general importance of further advances along these lines the intention is to proceed

nevertheless, yet once again the inevitable tendency is to diverge from the main theme of model validation. If the time-averaged salinity fields are to be seen as essential characteristics of the zonal current systems, in addition revealing indications of the precipitation influences which can take effect in the mutual temporal and spatial variations of the salinity associated with the currents, then this would be a highly relevant course to follow. Consequently in a manner similar to that adopted earlier in the EOF and Wavelet phase of the study a divergence is considered justified.

Within this context, the salinity field associated with the respective current was averaged in both vertical and meridional dimensions, and as a final product of this preliminary procedure this could be expressed as the temporal zonal distribution of the mean salinity associated with SEC(N), EUC and SEC(S). For reasons given earlier, it was not feasible to associate a saline field with the NECC. The statistical EOF technique was applied for the three salinity fields resulting from this procedure - the temporal zonal distribution of the mean salinity associated with respective currents. Table 4.3 presents the results of the three leading EOF modes, which account for 66%, 78% and 75% of total variance for the zonal salinity vertical-meridional averaged in the SEC (N), EUC and SEC(S) domains, respectively.

Table 4.3: Results of the first three main EOF modes for the zonal variation in time of the salinity field (vertical and meridional averaged) in the eastern equatorial Pacific Ocean current system.

	Variance (%)		
EOF mode	SEC(N)	EUC	SEC(S)
1	42	61	57
2	15	12	11
3	9	5	7

It is to be noted that the first EOF mode of the salinity field associated with the equatorial current system of the Pacific accounts for more than 60% of the total variance contributed by the group of three modes, leaving a minor residual to be shared by the other two modes. For this reason, and as previously expressed in the sequence of examinations in this study, there follows a phase, using the Wavelet transform, in which a decomposition procedure in the time-frequency domain is carried out so as to determine the dominant modes of variability, and to ascertain the manner in which these modes vary in time. This phase will concentrate upon the first EOF mode only.

Thus, the results of the Wavelet analysis (Morlet as mother wave, and $\omega_0 = 6$) when applied for the first mode of the time-series expansion coefficients as result of the EOF for the respective salinity field associated with the eastern equatorial currents, are presented in the Figure 4.13, 4.14 and 4.15 for South Equatorial Current - North branch (SEC(N)), Equatorial Under Current (EUC) and South Equatorial Current - South branch (SEC(S)), respectively.
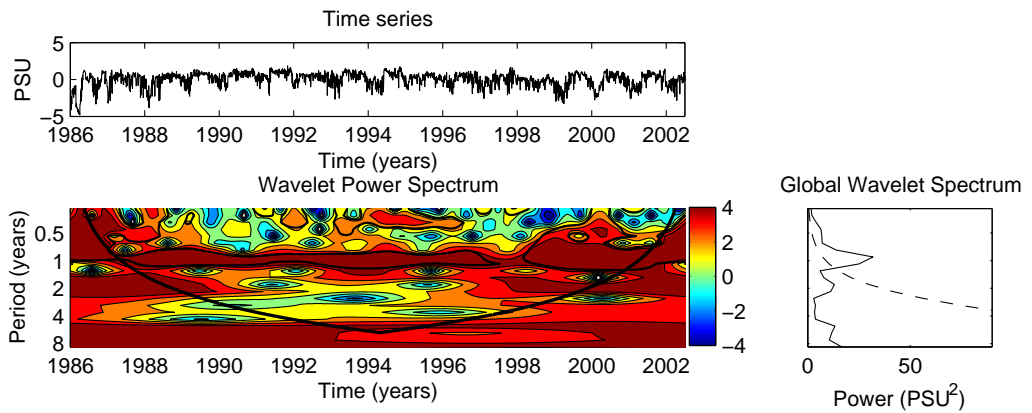
Figure 4.13: Result of Wavelet analysis when applied to the time series of expansion coefficients as a result of the first EOF mode of the zonal distribution of the mean salinity associated with the SEC(N). Time series of the zonal distribution of the mean salinity associated with the SEC(N) is shown in the top panel, the contour of wavelet power spectrum in the middle panel, and the global wavelet power spectrum in the right panel. In the right panel, the dashed line represents the confidence level of 95%. The contour wavelet power spectrum levels are chosen so that 75%, 50%, 25%, and 5% of the wavelet power is above each level, respectively. The dark line indicates the Cone of Influence (COI).
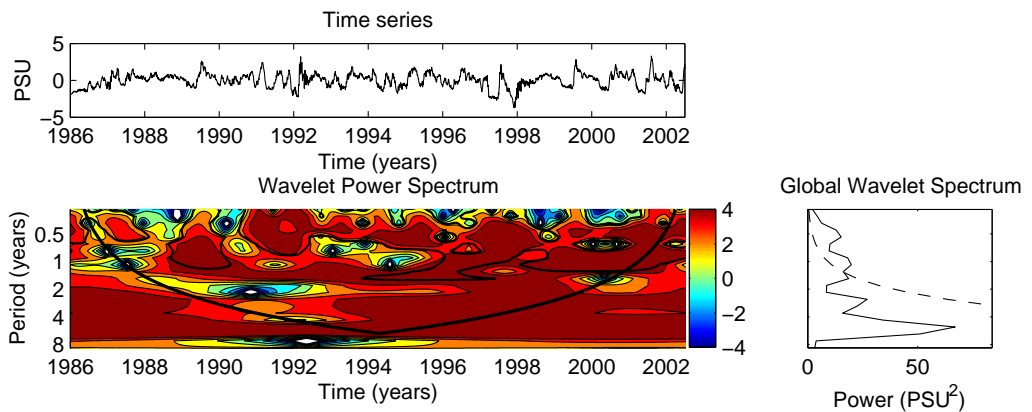

Figure 4.14: Same as Figure 4.13 but for the mean salinity field associated with the EUC.
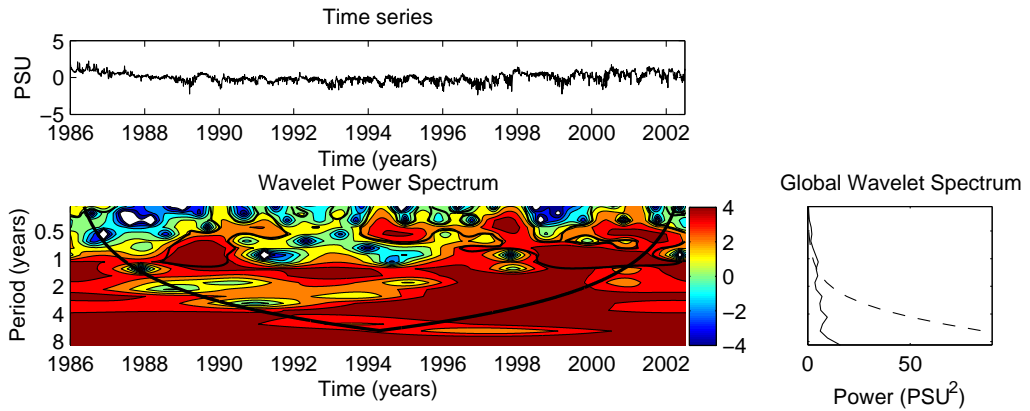
Figure 4.15: Same as Figure 4.13 but for the mean salinity field associated with the SEC(S).

Being directly wind driven, the equatorial oceanic current system responds quickly to variations in the wind field (Gordon, 1986). Therefore, the SEC(N) is strongest in the boreal winter, and the SEC(S) is stronger in the boreal summer, according to the latitudinal migration of the ITCZ and its relations to the atmospheric cells of circulation (which were discussed in Part I of this study). This characteristic is far more evident in the time series associated with the northern branch of the SEC (Figure 4.13 - upper panel), while for its southern branch (SEC(S)) this feature presents a smaller signature (Figure 4.15 - upper panel). The strengthening of this signal in both time series stands out during El-Niño events, when the Hadley circulation (north-south) is reinforced by the weakness of the Walker circulation. The EUC (Figure 4.14) is subjected to the same wind pattern, but at the same time it is a subsurface eastward flux. The time series of the salinity field associated with the EUC suggests to be the combination of the effects of the wind and the north and south neighbouring currents, the SEC(N) and the SEC(S).

The SEC(N), by its geographical position (Table 4.2, on page 104), is under the "shade" of the time averaged position of the ITCZ (about 5°N). By this reason, it is expected that the salinity field associated with the SEC(N) holds the same temporal variability as the ITCZ. The contour wavelet power spectrum for the salinity associated with SEC(N) presents a clear annual cycle (the same periodicity of the ITCZ), which becomes evident in the middle panel (figure 4.13 - middle panel), and it is also representative in the global wavelet spectrum (Figure 4.13 - right panel).

With regard to the time scale of the variability of the salinity field associated with the SEC(S), it is possible to recognize from the same panel a weak trend to the annual cycle (Figure 4.15 - middle panel). Since the SEC(S) positioning thoughtout the year is always south of the Equator, which means that the SEC(S) is relatively far from the ITCZ, the salinity field associated with the SEC(S) seems to be highly influenced by the variability of the Southerly wind along the west coast of South America. It is worthy of note that the SEC(S) is fed at least in part from equatorial and coastal upwelling, both of which are much weaker and warmer during El Niño, which can explain the variability observed in the middle panel during the El Niño events. Then, it is not surprising to see the high time-scale variability presented in all panels of the Figure 4.15.

The contour wavelet power spectrum of the salinity field associated with the EUC (Figure 4.14 - middle panel) presents its maximum variance in simultaneity with El Niño events. The seasonal cycle is such that the EUC is saltier when the transport is largest, because the upper layers of the EUC, which are saltier, make up most of the seasonal variability. During an El Niño event there is some warming of the EUC in the eastern Pacific, owing to more near-surface eastward flow under the relaxed trades (Johnson *et al.*, 2002a; Sloyan *et al.*, 2003).

In summary, the process of validation of the numerical model to be adopted as an assured Control for subsequent applications has been achieved, despite the shortcomings of comparative data and the limitations of relevant publications. Where possible, model output has been checked against *in situ* measurements, and also derived parameters and other inferences consequent on the application of the model have been compared with the findings of other authors. In the process of validation, the power of the technique to explore new fields and to expand the boundaries of current knowledge in the field of time-space variability of the SSS and the association of salinity properties with the equatorial current system of the eastern tropical Pacific have been confirmed. As an additional benefit, a number of potential leads have been identified for later evaluation. With qualified confidence in the model established the proposal now is to proceed to address the topic of salinity entrainment into the mixed layer and the significance of the input of atmospheric freshwater into the mixed layer.

b) Salinity entrainment into the mixed layer

Moving on from model validation and with confirmation of its potential, it now becomes possible to concentrate with finer focus upon applications of the model to relevant aspects of marine physics, and initially it is appropriate to examine salinity entrainment into the mixed layer.

The salinity entrainment into the mixed layer is the process whereby the mixed layer incorporates the adjacent salinity immediately underneath the MLD. For this study, a salinity entrainment "event" was assumed which could be achieved by three possible existing conditions:

- Downward motion of MLD;

- Vertical salt transport associated with the vertical velocity; and,

- Combination of both (dual entrainment).

Using the current oceanic numerical model approach, a search was conducted for the requisite conditions associated with potential entrainment of salt from the base of the mixed layer. The time-averaged results of the computation with the necessary characteristics are presented in Figure 4.16.
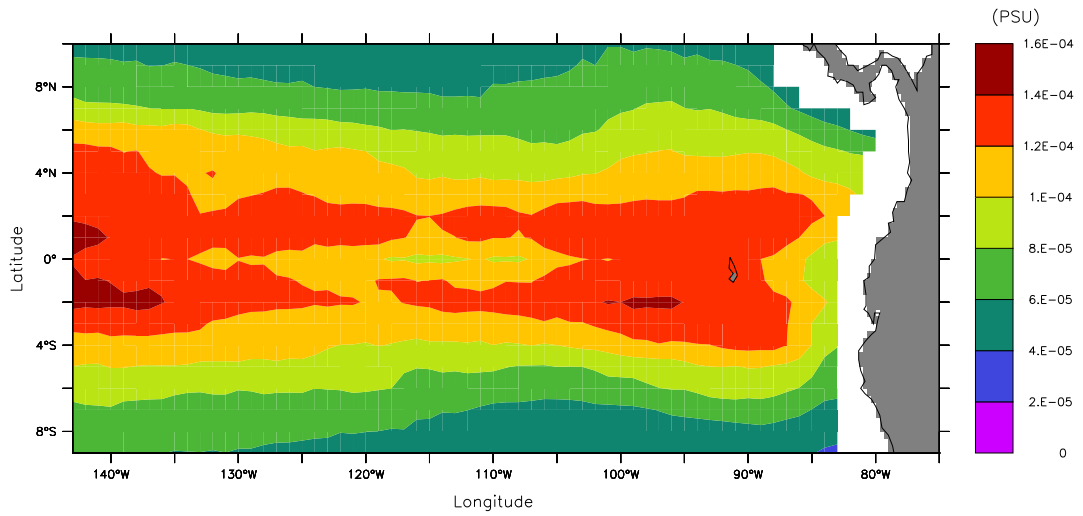
Figure 4.16: Mean salt entrainment (PSU) into the mixed layer through its base (averaged over the entire period).

It is worthy of note that the time averaged process of entrainment is concentrated in the equatorial region, and a first impression suggests that this feature is mainly dependent upon the Trade Winds but not in the direct sense and only after the divergent influence of Coriolis principles due to the Earth's rotation. It may be an exaggeration to say that the Coriolis effect is negligibly small near the equator, although small, it is still important. Thus, the Coriolis effect deflects the surface currents away from the equator on either side creating conditions suitable for the well-known equatorial upwelling.

Looking forward to understand the salt entrainment into the mixed layer on a time basis, an investigation was pursued based on the assumptions previously listed. For the positions in the Longitude 95°W at 3°N, 3°S plus the Equator, the results are shown in the Figure 4.17; also, in the same figure is over plotted the SOI signal in purple, which allows us to associate the connections between the salt entrainment and the ENSO cycle. The time series of the salinity entrainment along the 95°W indicates a link of this hydrodynamic process with the ENSO cycle.
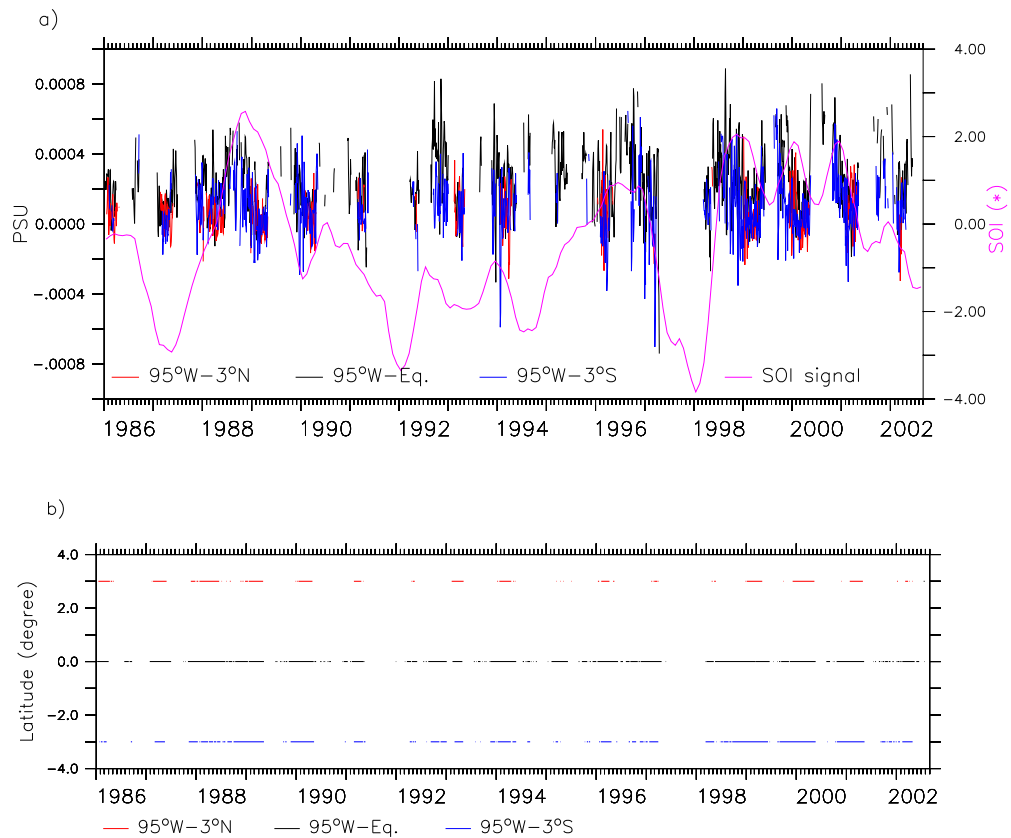

Figure 4.17: **Upper panel:** Time series of the salt entrainment (PSU) into the mixed layer from below along 95°W, for the Equator (black line) and Latitudes 3°N (red line) and 3°S (blue line). SOI signal is over plotted (purple line) for comparisons with the period of its occurrence. (*) SOI signal is based on the Trenberth method - monthly standard deviation and six months smoothed. SOI unit: hPa (1000 hPa subtracted). **Lower panel:** Latitude-time map of the occurrence of salt entrainment into the mixed layer through its base for 95°W-Equator (black line), 95°W-3°N (red line), and 95°W-3°S (blue line).

The time series of the salinity entrainment from below strengthens the idea raised by the preliminary analysis (the time-averaged salinity entrainment shown in the Figure 4.16), in which the salt entrainment is concentrated along the Equator (Figure 4.17 - lower panel). Therefore, it is possible to note from the same figure, in its upper panel, that exists the weakness or total suppression of the entrainment during El Niño periods (Figure 4.17 - upper panel). One of the remarkable characteristics of the El Niño event is the weakness of the Trade Winds, a consequence of which is to diminish the surface divergence of the equatorial waters, which are responsible for the equatorial upwelling. An additional consequence of equatorial upwelling is the upward displacement of the isotherms, which is implicitly related with the MLD. This upward movement would act in opposition to the entrainment, however, from the calculations carried out here, this effect is not capable of counteracting the effect of the upward movement of the waters. Then, it can be suggested with greater conviction that equatorial upwelling is the main feature responsible for the salinity entrainment into the mixed layer through its base in the region studied.

c) The significance of the flow of atmospheric freshwater

Now, in this concluding section of the oceanic model studies, the attention is drawn to processes whereby the atmospheric freshwater influences the SSS. In Delcroix *et al.* (1996) an approach was made to link the salinity and precipitation fields, based on the salinity samples obtained by the "ship-of-opportunity" program, with precipitation derived from satellite remote sensing via Outgoing Longwave Radiation (OLR). Those variables were spatially interpolated and monthly averaged for the tropical Pacific region and statistically analysed for the 1974-1989 period.

The purpose here is to introduce a new approach with significant differences from that reported by Delcroix *et al.*, and in this context, the intention is to include atmospheric flow of freshwater in its complete composition, i.e. as the resultant effect of precipitation and evaporation. The intention is to seek a more realistic and dynamic basis for an investigation of time variations of the SSS as modified by a contribution of atmospheric freshwater in its complete form. Note that Delcroix *et al.* did not consider the evaporation rate.

The numerical model was set up with the variable $(E - P)$ (evaporation minus precipitation) having the characteristic of an independent input. The precipitation and evaporation datasets were downloaded from the ECMWF-ERA40 data server, and interpolated so as to achieve the same spatial-time resolution as that of the hydrodynamic model, as described in the previous sections. And, within this context, a rework of the relationship between the time derivative of the Sea Surface Salinity (SSS) and the atmospheric flow of freshwater $(E - P)$ is addressed.

The chosen method aimed to achieve a map of correlation between the time variations of the salinity ($d(SSS)/dt$) in relation to the atmospheric flow of freshwater ($E - P$). Then, the correlation map between the $d(SSS)/dt$ and ($E - P$) is presented in the Figure 4.18.
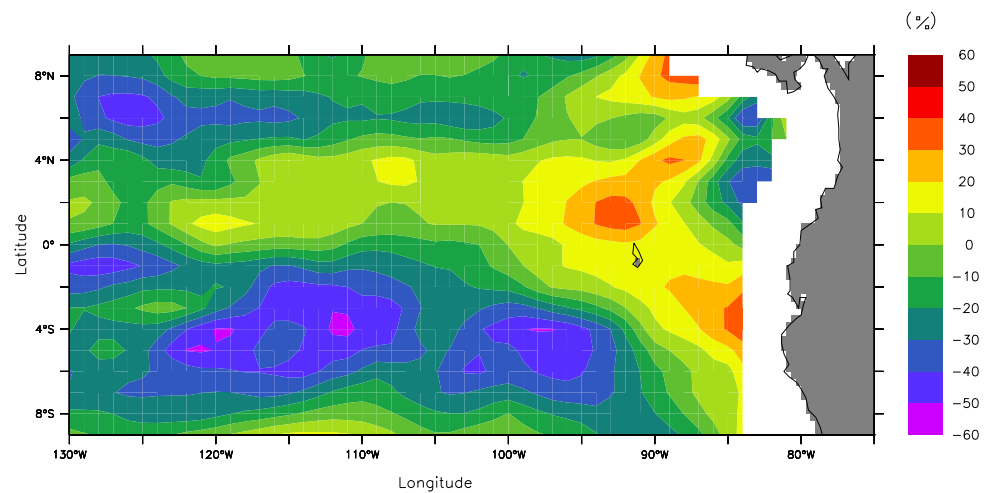

Figure 4.18: The correlation map between the time derivative of the Sea Surface Salinity, (SSS) ($d(SSS)/dt$), and the flow of atmospheric freshwater ($E - P$).

The map presents regions with high positive and negative correlations. Higher positive correlation is localized on the eastern Pacific Ocean, under the position of the ITCZ track, which confirms that the time variation of the SSS can be associated with the atmospheric flow of freshwater. Regions with lower correlation, or even negative ones, suggest that the temporal SSS's changes are the result of mixing or advection processes instead of being a major and straightforward response to the atmospheric flow of freshwater. These results are in accordance with the conclusions of Delcroix *et al.*, of which the most relevant at this is stage is the confirmation of the relationship between the SSS and ITCZ. Further discussion of the approach taken will be presented

in the following section.

With the significance of the association between the temporal variations of the SSS and the atmospheric freshwater input confirmed, it is proposed to recognize this as a satisfactory conclusion to the model applications of Part II. However there is a need to discuss and reflect on what has been achieved in the process.

4.3   Assessments and Reflections - Part II

The earlier sections of this chapter were initially dedicated to the analysis of the salinity field in the eastern tropical Pacific Ocean based upon an oceanic numerical modeling approach. Progress along these lines developed into a series of complementary studies leading to an overview of processes and distribution of salinity in the region, while simultaneously providing support and validation of the so-named "Control Run" (Ctrl), promoted in Part I as a key tool.

What now must follow is a formal assessment of the application of this tool to the distribution of salinity in the region and the relevant processes of change. This will take the following form:

- An assessment of the validation procedure;

- Consequent upon confidence gained by validation, to evaluate the process of salinity entrainment into the mixed layer via its base;

- To consider the temporal variations of the Sea Surface Salinity as a direct response to the atmospheric freshwater flux, and

- To conclude by acknowledging the significance of the above analyses.

Validation of the "Control Run"

The validation of the Ctrl was forced using the precipitation and evaporation supplied by ECMWF-ERA40 and the temperature and velocity field supplied by MOM2. The time series of the SSS (Figure 4.1, on page 88) and the time series of the depth of the Z20 (Figure 4.3, on page 93) were compared with *in situ* data, provided by the buoys of the TAO/EPIC array of NOAA.

Concerning the comparison between the SSS and *in situ* data, it is worthy of note that the estimated time series of SSS by the numerical approach relies strongly on the combination of the precipitation and evaporation rates (Equation 4.1, on page 84), but if the evaporation rate presents a field which is fairly constant, in contrast, the diagnostic variables, such as precipitation present a large variability in the tropical oceanic regions (Trocoli & Kållberg, 2004), thus, in consequence, a close agreement between the SSS as output of the Ctrl with *in situ* data was not reached in the high frequency spectrum by the reasons as described in Tomczak (1995). However, the long term and trends were well represented, which could be verified when the salinity field was integrated over the entire volume domain. This latter result shows that the salinity in the model retains a relationship with the ENSO signal (Figure 4.2, on page 90).

With regard to the comparison between the time series of the Z20 produced by the Ctrl using the *in situ* data, agreement was reached for both the regions of the frequency spectrum, the low and the high frequencies. In addition, the vertical section along the Equator for the time-averaged temperature field (Figure 4.10 - lower panel) presents the expected inclination of the isotherms, which is a potential representation of the observed upwelling in the easternmost tropical Pacific.

Moreover, validation of the Ctrl was carried through not only by comparisons with *in situ* data, but complementary studies had also been made based on derived parameters from the oceanic model with previous studies published by other researchers. Using the model output includes the analysis of the time-space variability of the SSS, as well as that due to volume transported by the main oceanic currents of the equatorial eastern Pacific Ocean. The latter mentioned methods of validation differ from straightforward comparison of the model output with *in situ* data, and they are argued individually as follows.

Initially, the time-space variability of the monthly mean of the SSS was anal-ysed by the EOF technique and compared with previously published statistical studies. Among them, can be cited: firstly, Delcroix & Henin (1991) then Delcroix *et al.* (1996) where statistical approaches were employed in the investigation of salinity and precip-itation relationships for tropical oceans; and finally, in Delcroix (1998) is presented a comprehensive statistical study of variability in the tropical Pacific.

When limiting the studies of the time-space variability of the monthly mean of the SSS to the EOF analyses, the studies developed here strongly agreed with the above quoted works, but it is appropriate to keep in mind that, in the present work, an extra concept was given to the time series of the expansion coefficients derived from the EOF analysis, with the intention to achieve a better understanding of the time-frequency variability of such signals. Then, as consequence of the new approach, the individual results for each leading mode of the EOF when applied to the monthly mean of the SSS, are presented simultaneously in the relevant study referring to the time-frequency variability of the signals (achieved by the Wavelet analysis), as follows.

The first EOF mode accounts for 35% of the total variance of the monthly mean of the SSS. The first spatial EOF mode presented a zonal structure (Figure 4.4 - upper panel) that differes only in the easternmost Pacific Ocean, where there is an intense gradient of the variability near to the western Central America coast, and al-most parallel to it. The main zonal structure of the spatial pattern presents its more intense gradient under the mean position of the ITCZ, so dividing the ocean basin, as a dipole structure, into two parts in the vicinity of 5°N. Another noticeable feature is the most negative homogeneous correlation (up to -30%) located in the easternmost region of the tropical Pacific. The main candidate as an explanation of such a feature could possibly be the wind jets associated with the three major gaps in the Central American Cordillera. Since the wind jets present as their main characteristic significant variability in timing and intensity (Kessler, 2006), they have the potential to create

multi-layered changes in the salinity field and displaying non-regular frequency.

In a search for further evidence to support this concept, time-dependency characteristics associated with the first EOF mode, were examined by the Wavelet analysis of the expansion coefficients (Figure 4.4 - lower panel). Here interest is expressed in certain features of the analytical output. In the case of the only signal giving a 95% confidence level, the annual signal, (Figure 4.7 - lower panel) considerable interest is displayed in terms of its discontinuities. The signal appears to collapse after periods of approximately three years continuity, displaying a non-steady cycle only overcome by the last strong El Niño event (1997/98). Otherwise the signal appears to experience an increase of variance at 1-8 years periodicity. This intermittent annual signal could be related to a combination of the ENSO effects with the migration of the ITCZ. Although the techniques adopted here were pivotal to the identification of the existence of these characteristics, their ability to advance to a full explanation of the processes involved was naturally limited.

Now turning to the second leading mode of the EOF analysis based on the monthly mean SSS time series, we note that it demonstrates a spatial pattern (in Figure 4.5 - upper panel) with its most prominent feature being a higher positive variance feature suggesting a shadow of the northern hemisphere Trade Winds path, extending from the Central American Isthmus to the 110°W Longitude. Visually there appears a temporal variation with a period of approximately 8 years with interannual oscillations (Figure 4.5 - lower panel). However the Wavelet analysis assigned a 6 years period to the feature (Figure 4.8 - middle and right panels). Then further speculation can be made on the basis of observation of the limit regions in the same panels (Figure 4.8 - middle and right panels). They imply signals at approximately 10 years, virtually on the margin of competence far such a short observational record. In summary, since the Wavelet technique suggests responses of 6 and 10 years, this may be seen to corroborate a signal of 8 years reported earlier as a combination of the former two periods. The

second EOF mode accounts for 13% of the total variance.

The final third EOF mode produced by the analysis of the monthly mean SSS accounts for just 7% of the total variance. Its spatial pattern indicates a dominant equatorial characteristic (Figure 4.6 - upper panel) and the associated time series of its expansion coefficient presents a negative correlation of -61% with its equivalent for the first mode. Based on the properties of the EOF analysis, which assumes the uniqueness of modes, the third mode suggests a classical case of degeneracy of eigenvalue. If there is more than one linearly independent eigenvector for a given eigenvalue we say that the eigenvalue in question is degenerate (*Anonymous*, (1967); North *et al.*, 1982). Where degeneracy occurs it is almost always related to some spatial symmetry of the system (Solbrig *et al.*, 2005). However, the degenerate subspace is a vector space, it is possible that compatible observables admit a basis of simultaneous eigenvectors. Even though, the Wavelet analysis served to underline their spatial similarities. In spite of its low significance (7% of the total variance), this weak signal nevertheless is seen to be an established characteristic modal feature. Such linked general spatial symmetries are sometimes distinguished by the term "accidental degeneracy".

What is clearly demonstrated in this procedure is that the basic analysis of the monthly mean series of the SSS by the EOF principles is found to be in agreement with previously published work and in so doing gave support both to concepts adopted here and also to the growing consensus of opinion as to the interaction of regional conditions. Nevertheless, much more has been achieved. The Wavelet technique of analysis applied to the time series of the expansion coefficient of each EOF mode has provided much more than the basic EOF procedure can achieve in its own right. In the first place it has confirmed the results of the earlier EOF process, but more importantly it has opened a window enabling an advancement of knowledge of the time-space variability associated with these individual modes, not previously seen. That these new concepts offer an immediate relationship to known geographical and environmental features is

both an added bonus but also provides a potential additional tool to assist in the diagnosis of freshwater sources.

Following an acceptable validation of the Ctrl, permission was given to proceed with the application of the Active Tracer Model as a validated tool and the early application addressed the volume transport of the main currents of the equatorial eastern Pacific. Here the definition of the currents adopted the proposals of Johnson *et al.* (2002b), based upon characteristic water properties. Since the domain of the model did not extend polewards beyond 10°N, it was considered inappropriate to include the NECC and its associated salinity. Consequently analysis was restrained to EUC and SEC in both its north and south branches. The volume transported by those currents strongly agreed with previous studies (e.g. Kessler *et al.*, 2003). The agreement, in fact, was sufficient to prompt the opportunity to expand regional knowledge of the salt transport for which these ocean currents are responsible, yet noting that a boundary had been imposed in the current work at 90°W Longitude due to the complexity of the current system to the east of that boundary. Kessler (2006) had first described its complexity and the influence of the three major gaps in the Central America Cordillera which, through wind jets, can alter the region's hydrodynamic circulation considerably.

In proceeding to examine the possible connection between the equatorial current system of the eastern Pacific and the associated salinity properties, caution was required due to the paucity and patchy nature of *in situ* data, or, in fact of previously existing analytical literature. Consequent limits to the model validation had to be kept in mind, yet the opportunities afforded overcame the difficulties.

The zonal time averaged mean salinity associated with the equatorial current system of the Pacific presented a gradient of increasing salinity values from the easternmost Pacific towards the date line (Figure 4.12), for any one of the three currents which were being treated in the analysis (this study and Johnson *et al.*, 2002b).

Such characteristic, in addition to the study carried out in Part I in relation to the time-space variability of the precipitation in the eastern region of the tropical Pacific Ocean, motivated the analysis of the temporal variability of the salinity associated with those currents. An investigation was pursued with regard to the salt variability of the equatorial eastern Pacific current system, which, generally, presented three major periodicities: intra-annual (∼6 months), annual, and ENSO scale. The case for each current system is argued as follows.

In the analysis of the salt variability in the north branch of the South Equatorial Current, SEC(N), (Figure 4.13 - upper panel), a very strong annual cycle was displayed. Then reference to the SOI record confirms that clear indications of El Niño conditions appear for 1986/87 and 1997/98. The analyses show that for the SEC(N) the El Niño years presented anomalous salt variability over periodicities from 6 months to 2 years for the first event and much broader for the second event ranging from 6 months to 8 years.

Addressing now the South Equatorial Current - SEC(S), reference to Figure 4.15 immediately indicates that its variability is more complex than that which was seen in its northern equivalent. There are perhaps many reasons for this to be so. For example this feature could be related to the weakness of the SEC(S) by comparison with the SEC(N). Figure 4.10 provides an evaluation of the volume transport in both cases from which the difference can be seen, noting that the vertical scales are not uniform. Then SEC(S) receives a wind-driven contribution from those Southerly Winds from the South American coastal zone which themselves have a large spatial and temporal variability. It may be argued that this feature is supportive rather than otherwise of the main theme of this study, namely that the high temporal variability in the salinity of the SEC(S) (in this case) carries the characteristics of its source i.e. the influences of its atmospheric origin in terms of significant temporal variability. Reference to Figure 4.15 - upper panel, clearly shows this typical variability in its time series despite its weak

amplitude. Then El Niño conditions are essentially associated with a reinforcement of the Southerly Winds of the higher latitude coastal zone and a decrease in the Trade Winds of the eastern Pacific creating temporal change in the consequent salt content. The end result of these processes can be seen in Figure 4.15 (middle panel) for the El Niño years, 1986/87 and 1997/98.

The third major equatorial current contemplated in this work - Equatorial Under Current (EUC) - located as it is in the latitudes between the two branches of the SEC carries their characteristic temporal signatures as a relevant aspect. The interannual and annual cycles are well pronounced as is the Southern Oscillation Index (SOI), all of which are to be seen in Figure 4.14 - right panel. During El Niño events (1986/87 - 1991/92 - 1997/98) the EUC becomes weak, or in fact may disappear completely, adding to the variability of salinity visible in Figure 4.14. It has also been shown that the EUC is prone to lose volume from its successive denser and deeper layers (Sloyan *et al.*, 2003), which is suggested to be a factor in the temporary disappearance of the EUC at the time of El Niño enhancing the apparent variability in the statistical analysis of salt.

Sometimes comparing the output of the Ctrl model run with *in situ* data, sometimes comparing with results of previous works, the model was considered to have arrived at a state of trustworthiness of skills appropriate for the oceanic numerical approach matched to a potential to advance into a diagnostic role. The intention was to apply the technique to address problems, support hypotheses already raised and to compare with the output of the more conventional approaches of others. Again, during the progress of validation of the SSS other opportunities arose to take a brief digression on the basis of what had been achieved but outside the validation target: a) To perform an intensive investigation of certain features where conventional methods had failed to provide a convincing understanding of the operating physics, and b) to pursue the matter of salt transport time variability by the main current systems of

the Eastern Pacific Ocean. Although a digression from the main theme, these topics served to add further confidence in the efficiency of application and the potential for diagnosis of the numerical model.

Then, in the context of the further investigation of the potential of the oceanic model and with the intention to amplify knowledge of the salinity in the upper layers of the eastern tropical Pacific Ocean, two more analyses were carried out using the model. The achievements of the latter are argued as follows.

Salinity entrainment into the mixed layer

The first investigation carried out with the intention to fill a gap that until now had not been addressed in the region was the salinity entrainment into the mixed layer, via its base. To achieve such intent, it was assumed that the salinity entrainment from below could occur by the downward motion of MLD, or by the vertical salt transport associated with the vertical velocity, or by the combination of both (dual entrainment). As a result of this assumption, the salt entrainment, when averaged for the entire period of study, was found to be concentrated in the equatorial region (Figure 4.16, on page 118), and this result can be primarily explained by the equatorial upwelling, and also as a consequence of the convergence into the EUC (Wyrtki, 1981; Lukas, 1986; Bryden & Brady, 1985; Pedlosky, 1988; Gu & Philander, 1997; Kleeman *et al.*, 1999; Sloyan *et al.*, 2003; and Kessler, 2006).

The time-averaged salinity entrainment was able to explain most of the frequencies of the occurrence of such physical process, however, an inquiry was carried out in order to provide evidence of salinity entrainment into the mixed layer from below on the basis of its temporal distribution. To enable this study with particular reference to the region of interest, three latitudes were selected along the 95°W Longitude so as to define a study case. These were 3°N, 3°S, and the Equator itself. Based on the

same above premises for the occurrence of salt entrainment, the time series of salinity entrainment into the mixed layer in the Longitude 95°W at 3°N, 3°S and the Equator were presented in the Figure 4.17 (Page 119). The main feature of this diagram is the weakness, or in fact absence, of saline intrusions into the mixed layer from below during the El Niño periods. Thus, becomes worthy of comment that one of the essential characteristics of the development of the El Niño event is the weakness of the Trade Winds of the eastern Pacific, which simultaneously suppresses equatorial upwelling and pushes downward the isotherms (and implicitly, the MLD). These features of the El Niño suggest that the combination of the deepening of MLD in the eastern Pacific Ocean (which is favorable to the salt entrainment into the mixed layer) jointly with the upwelling weakness (acting against the salt entrainment) are strong candidates to help sustain a barrier for salinity entrainment through the bottom of the mixed layer. From the current modeling approach, the deepening rate of the MLD was not strong enough to compensate for the reduction of the upwelling observed in the El Niño events. Furthermore, it is important to point out that the region has peculiar interacting characteristics that make the region dynamically puzzling, and as examples of the main factors that intervene with the hydrodynamics of the region, they can be cited as the cold tongue, Ekman pumping, and the time variability of the MLD associated with the ENSO cycle (e.g. Johnson *et al.* 2002a, b; Sloyan *et al.*, 2003; McPhaden, 2004; Garcés-Vargas *et al.*, 2005; and Kessler, 2006).

The influences of the flow of atmospheric freshwater

Finally to conclude the assessment of the oceanic model, reference is made to the relationship observed between the time derivative of the Sea Surface Salinity and the atmospheric freshwater flow (evaporation minus precipitation). This physical interaction is investigated through the correlation between the field of the $dSSS/dt$ and that of the $(E-P)$. The correlation map of the influence of the flow of atmospheric freshwater in the SSS through the time derivative of SSS is given in the Figure 4.18 (Page 122).

It is well known that the Pacific Ocean under the ITCZ and its equatorial region have a very high precipitation rate, and as a result, the eastern tropical Pacific presents the lowest SSS in its basin. Thus, it is therefore hardly surprising that this characteristic, in a more limited regional sense was replicated by the model which demonstrated the highest correlation index. Alternatively, negative and lower correlation values on the outer fringe of the ITCZ "shade" suggest that advection and the mixing processes are more important than the influence of the flow of the atmospheric freshwater. Furthermore, two regions in the extreme eastern region, where the correlation map presented negative values, are coincident with the positive wind stress curl upwelling in the northern hemisphere - Figure 1, *in:* Kessler, 2006 - bringing in salt of the sub-thermocline water, which suggests that the influence of the atmospheric freshwater can be diminished in those particular regions. Furthermore, Wijesekera *et al.* (2005) suggest that those anticyclonic eddies influence the transport of the heat and salt westward from the region.

To summarise this section, an oceanic model has been presented which combines the widely-used numerical hydrodynamic model (The Modular Ocean Model, Version 2 - MOM2), with the mixed layer model so as to provide a "hybrid package" to target the complex interactions of water properties and global ocean circulation in a unique equatorial environment. The Model has presented itself as a reliable tool to apply to these regional circumstances, and the achievements of this work can be identified in the list which follows.

- The Sea Surface Salinity (SSS) does not exactly match the high frequency of the *in situ* observed data, but the seasonal and annual trends were well reproduced. Furthermore, the spatially integrated salinity for the entire volume of the domain displays a clear relationship with the SOI. Moreover, the time-space variability of the monthly mean of the SSS agreed with previous studies; in addition the present work offers an important advantage in relation to the others when considering

the dependence of the time-frequency of the main modalities of the oscillations of the SSS.

- The depth of the 20°C isotherm (Z20) is well represented in both high and low frequencies, and the section along Equator for the mean temperature shows the representative inclination of isotherms referring to the observed upwelling in the eastern Pacific.

- The section along the Equator for the mean zonal velocity shows characteristics of the EUC termination in the eastern Pacific Ocean.

- The volume transport associated with the three main equatorial oceanic currents covered in the domain of this study (EUC, SEC(N) and SEC(S)) presented very good agreement with previous works.

- The mean salinity associated with the main current system of the equatorial Pacific is well represented and it is in agreement with previous published studies.

- The saline fields associated with each one of the currents above cited disclose that their variability maintains a relationship with the main atmospheric phenomena which reach the region (e.g. ENSO and developments associated with it).

- In addition to the association between the salinity fields and the major current system, salt entrainment into the mixed layer through its base also presented a relationship to the atmospheric phenomena as evidenced along Longitude 95°W for latitudes 3°N, 3°S and also for the Equator.

- The time derivative of the SSS, when related to the flow of the atmospheric freshwater, was shown to be robustly connected with the ITCZ.

Finally, the set of results achieved by diverse methods of validation and analyses gave the necessary confidence to assume the numerical modeling approach to be well skilled and reliable, and therefore, validated for use as "Control Run" (Ctrl) for the associated work already quoted in Part I. Additionally, the complementary analyses added more substantial understanding of the salinity in the upper layers of the eastern tropical Pacific Ocean.